Spectral Properties and Heterogeneity of Phobos from Measurements by *Phobos 2*

SCOTT MURCHIE

Applied Physics Laboratory, The Johns Hopkins University, Laurel, Maryland 21771
E-mail: scott_murchie@jhuapl.edu

AND

STEPHANE ERARD

Universite Paris-Sud, 91405 Orsay, France

Phobos 2 observed parts of the surface of Phobos with three multispectral sensors covering the wavelength range 0.33–3.16 μm. These included a CCD camera (VSK) with two channels covering visible and near-infrared wavelengths, an ultraviolet–visible point spectrometer (KRFM) covering the 0.33–0.60 μm wavelength range, and a near-infrared imaging spectrometer (ISM) covering the 0.76–3.16 μm wavelength range. We have rederived the calibrations of all three data sets, using consistent methodologies in which known regions of Mars observed by the instruments serve as spectral standards. All three data sets yield mutually consistent results, and where the *Phobos 2* observations overlap previous measurements they are closely consistent.

The observed portion of Phobos is spectrally heterogeneous and consists of two fundamental spectral units. A "redder unit" with a visible/near-infrared color ratio of 0.6–0.85 covers most areas that were observed at high resolution by the *Viking* orbiters. Its visible-wavelength albedo is generally low, 6–7% in dark intercrater regions, but the rims on fresh craters are brightened by up to 40% without a change in color. Spectrally the redder unit exhibits a strong red slope at all wavelengths, with a steeper slope below an inflection at 0.5 μm. There is little or no absorption due to H_2O at 3 μm, indicating a nearly anhydrous surface composition. There is however a weak mafic mineral absorption at 1.0 μm, which increases in strength in progressively less red areas. The reddest material with the weakest 1-μm absorption is exposed in several small, dark-floored craters, which previously have been interpreted as local concentrations of impact melt. A "bluer" unit with a visible/near-infrared color ratio of 0.85–1.2 makes up the interior and ejecta of the large crater Stickney. This unit is typically darker at visible wavelengths (albedo 5–6%) and it lacks the brightened crater rims typifying the redder unit. In contrast to the redder unit, in the bluer unit albedo and color are correlated; the brightest (albedo ~8%), bluest materials occur on the walls and rim of Stickney. The bluer unit exhibits a shallower falloff of reflectance below 0.5 μm than the redder unit, but its near-infrared properties are unknown. Spatial distributions of the units show that the bluer unit originates at depth, and that the redder unit is a surficial layer.

Only the redder unit is well enough characterized spectrally for detailed analysis. Its spectral heterogeneities are inconsistent with simple particle size differences, and suggest the presence either of distinct lithologies or of a single lithology affected to different degrees by "space weathering." It is distinct from the C and D asteroid classes with which Phobos has commonly been compared, and most closely resembles T-type asteroids or highly space-weathered mafic mineral assemblages. It is also distinct from most previously proposed meteorite analogs. Several models can explain the properties and spatial distributions of the two spectral units. Phobos's surface material may be rich in mafic minerals, and affected to different degrees by space weathering. Alternatively, Phobos's surface could consist of a mixture of mafic-poor material (possibly resembling D asteroids) and mafic-rich material. In view of the moon's low density (1.9 ± 0.1 g/cm³), a high mafic mineral content would imply substantial internal porosity. © 1996 Academic Press, Inc.

INTRODUCTION

The martian satellite Phobos is the best-studied small body in the solar system. High spatial resolution imaging by *Mariner 9*, *Viking 1* and *2*, and *Phobos 2* has provided detailed information on the satellite's shape, surface morphology, and albedo features. Terrestrial telescopic data and measurements from the *Mariner 9* UV spectrometer, the *Viking lander* cameras, and the Hubble space telescope have been used to determine disk-integrated spectral properties. Several groups have used such measurements as the basis for identifying possible meteorite analogs to Phobos's surface material. More recently, disk-resolved multispectral data from *Phobos 2* have revealed a spectrally heterogeneous surface. These types of information are important

to addressing the questions of Phobos's composition, lithologic heterogeneity, and geologic evolution. In a larger sense, though, detailed knowledge of the surface of Phobos is critical for comparative geologic studies of small bodies. High spatial resolution imaging and spectroscopic data from spacecraft have recently been returned for the asteroids 951 Gaspra and 243 Ida from *Galileo* (Belton *et al.* 1992, 1994, Granahan *et al.* 1994, 1995), and are anticipated for 433 Eros from *NEAR* (Veverka *et al.* 1995). Despite similarity in size, unlike the latter bodies Phobos orbits Mars as a natural satellite. Comparison of Phobos with those asteroids may thus help shed light on the importance of orbital dynamics and position of the solar system to the geologic evolution of a small body.

Physically, Phobos is irregular-shaped, low in density, and highly cratered. Phobos's shape can be approximated as an ellipsoid having principal axes of 27 km, 22 km, and 19 km (Duxbury and Callahan 1989). However, there are significant local departures from this approximation, due to occurrence of quasi-planar "facets" several km in size separated by low, quasi-linear "ridges" (Thomas 1978, 1979). Determinations of satellite mass and volume lead to an estimated density of 1.9 ± 0.1 g/cm^3 (Avanesov *et al.* 1989, 1991). Geology of the surface is dominated by craters ranging in size up to 10 km in diameter for Stickney, the largest crater on the satellite (Fig. 1a). The craters occur in a variety of states of degradation but only Stickney exhibits unambiguous evidence for significant ejecta deposits, located proximal to the crater rim to the southwest (Fig. 1a) (Murchie *et al.* 1991a).

Prior to the *Phobos 2* mission, the highest spectral resolution measurements of Phobos were the composite spectrum assembled from *Mariner 9* UVS, telescopic, and *Viking* lander camera observations. Different wavelength ranges of the composite spectrum represent different viewing geometries that covered the sub-Mars and leading hemispheres (Pang *et al.* 1978, Pollack *et al.* 1978). At visible wavelengths this composite spectrum is flat or spectrally neutral, and reflectance falls off markedly at wavelengths $<0.4 \mu m$ (Fig. 2). Geometric albedo at visible wavelengths has been estimated as 0.066 ± 0.006 (Klaasen *et al.* 1979), 0.05 ± 0.01 (Veverka and Burns 1980), and 0.07 ± 0.01 (Pang *et al.* 1983). These "average" spectral properties resemble those of C-type asteroids. The highest spatial resolution color measurements, 3-band *Viking* images (0.44, 0.53, 0.59 μm), covered primarily the trailing hemisphere and did not reveal major heterogeneities (Veverka and Duxbury 1977).

The apparent spectral shape and homogeneity of Phobos were interpreted to indicate that Phobos has a well mixed surface composed of carbonaceous chondrite (e.g., Pang *et al.* 1978), inferred to be the primary constituent of many C-class asteroids. Carbonaceous chondrites are not thought to have condensed from the solar nebula at Mars's

distance from the sun, so such a composition for Phobos may imply an origin as a captured body (cf. Burns 1992). Many carbonaceous chondrites are water-rich, so this interpretation has also been invoked in suggestions that Phobos could serve as a source of hydrogen and oxygen for a human Mars mission. Although the carbonaceous chondrite interpretation is deeply engrained in literature on the subject (e.g., Thomas *et al.* 1992), Britt and Pieters (1988) pointed out that the limited disk-integrated spectral data are fit equally well by water-poor "black chondrites," ordinary chondrites which have been darkened by regolith processes. Ordinary chondrites are thought to have originated in the inner solar system, so such a composition for Phobos would not necessitate an exotic origin.

In monochrome *Viking* orbiter images Phobos exhibits substantial albedo heterogeneity. Fresh craters commonly have materials on their rims and walls that are up to 30% brighter than surrounding surfaces when viewed at phase angles $<30°$, though they are undistinguished at much higher phase angles (Fig. 1b) (Thomas 1978, 1979, Avanesov *et al.* 1989). Similar brightened materials occur on local topographic highs including the low, quasi-linear ridges (Thomas 1978, 1979). Reflectance properties of these "bright rims" and "bright ridges" have been attributed to photometric effects of surface texture (Thomas 1979) or to differences in the relative abundances of low- and high-albedo components (Avanesov *et al.* 1991, Shkuratov *et al.* 1991). Other craters have floors that appear darker than surrounding surfaces, especially when viewed at phase angles of $\geq 30°$. Such "dark-floored craters" have previously been interpreted as having a rough surface texture due to porous impact melt (Goguen *et al.* 1978).

Measurements by the multispectral detectors on *Phobos 2* reveal that Phobos's surface also exhibits a factor of 2 variation in visible/near-infrared (NIR) color, and they provide high spectral resolution measurements of restricted regions. Two-color images from the VSK camera cover ~60% of the surface in the 0.4–1.1 μm wavelength region. These show that on average the surface is somewhat reddish, that the interior of Stickney exposes relatively "blue" material, and that dark-floored craters consist of a relatively "red" material. "Bright ridges" and "bright rims" are brightened relative to their surroundings with little or no change in color (Avanesov *et al.* 1989, 1991, Murchie *et al.* 1991a). The disk-averaged geometric albedo is estimated as 0.068 ± 0.007 (Avanesov *et al.* 1991). Spectra from the KRFM point spectrometer cover visible and near-ultraviolet (UV) wavelengths; these also show substantial local color differences (Ksanfomality *et al.* 1989, 1991, Murchie *et al.* 1991a). NIR spectra from the ISM imaging spectrometer reveal a 1-μm absorption whose strength varies laterally by several percent (Bibring *et al.* 1990, Langevin 1991, Murchie *et al.* 1991b, Murchie and Erard 1993), and that Phobos exhibits little or no H_2O absorption at 3.0 μm

FIG. 1. (a) Viking image 252A15, showing bright crater rims and intervening darker plains in the trailing hemisphere. The scene is approximately 10 km across, and corresponds to the western part of the left VSK image in Fig. 3a. (b) *Viking* image 87A52 showing the leading hemisphere, with the crater Stickney and the region to its west and southwest. The scene corresponds approximately with the part of the surface shown in the right image in Fig. 3a.
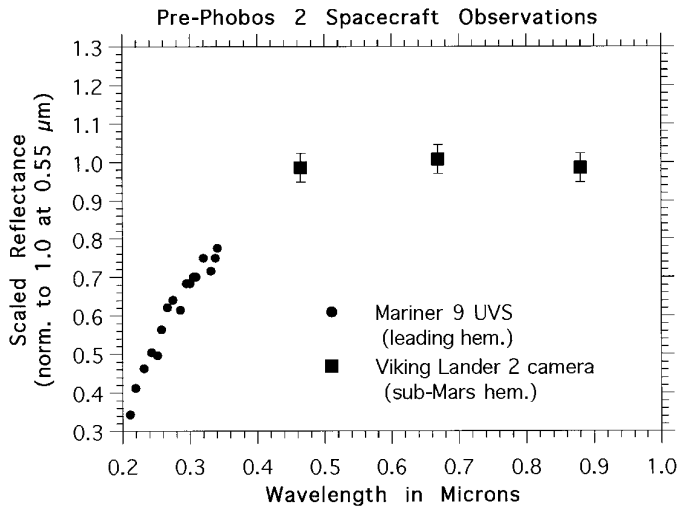
FIG. 2. The composite spectrum of Phobos presented by Pollack *et al*. (1978) and Pang *et al*. (1978). Different portions of the spectrum are derived from measurements of different parts of Phobos's surface.

(Bibring *et al*. 1990). The results from *Phobos 2* do not support the concept of a homogeneous, water-bearing surface composition, but show instead that surface composition and its relationship to geology are unexpectedly complex.

The measurements from *Phobos 2* have unfortunately been less informative, so far, about the absolute spectral properties of Phobos's surface and what they imply about mineralogic composition. This difference arises because spectral heterogeneities are recognizable based solely on internal variations within each data set, whereas absolute spectral properties and inferences about mineralogy require consistent data calibration and, preferably, merging and intercalibration of the individual data sets to synthesize broader wavelength coverage. Two groups have attempted this synthesis. Bibring *et al*. (1991) and Ksanfomality and Moroz (1995) attempted to calibrate each data set independently using different methodologies, and then to merge them to derive continuous spectral coverage. Murchie and Erard (1993) and Murchie and Zellner (1994) intercalibrated KRFM and ISM data using the VSK imagery as a link, but they also used different methodologies in reducing the individual data sets. Not surprisingly, these attempts yielded differing results.

In this paper we describe how we have reprocessed the data from *Phobos 2*, intercalibrated the different data sets, and used them to determine the spectral properties and spatial distributions of materials composing Phobos's surface. First, we review the multispectral data returned from *Phobos 2*, and explain which portions of it we have used and why. Second, we describe how measurements of Phobos in all three data sets have been calibrated using the same standards, observations of known regions of

Mars, and how the data sets have been intercalibrated using their overlapping wavelength coverages. We show that the calibrated *Phobos 2* data are highly consistent both with each other and, where the spatial coverages overlap, with independent measurements acquired by *Mariner 9* and the Hubble Space Telescope. Third, we document the spectral properties and spatial distribution of materials on Phobos's surface. We show that the surface contains two distinct spectral units, one consisting of the interior and ejecta of Stickney and the other consisting of the remainder of the surface. Fourth, we compare Phobos with other low-albedo small bodies and with analog materials. We show that Phobos is distinct from most low-albedo asteroids such as C- and D-types, and that its surface composition is anhydrous or nearly so. Finally, we use these results to speculate on Phobos's composition and internal structure.

DATA ACQUIRED BY *PHOBOS 2*

The *Phobos 2* mission plan included three preliminary encounters with Phobos at a distance of several hundred kilometers, while the spacecraft orbited Mars in its equatorial plane. During each of these encounters, in February and March 1989, multispectral measurements were acquired to characterize large-scale albedo and spectral properties of the surface. Subsequently the spacecraft was to have approached to within 50 m of Phobos, emplaced landers, and conducted intensive remote sensing of a small part of the surface. Loss of spacecraft signal after return of data from the third preliminary encounter limited the scientific return of the mission, but still provided spectral measurements of Phobos at far higher spatial and spectral resolution than had been obtained previously.

Three multispectral sensors returned data on Phobos during these encounters. The data characteristics are summarized in Table I. VSK (Videospectrometric Camera) consisted of two wide-angle CCD cameras having bandpasses of 0.4–0.6 and 0.8–1.1 μm, a broadband 0.4–1.1 μm narrow-angle CCD camera, and a 35-channel spectrometer designed to return 0.4–1.1 μm spectra of each scene imaged (Avanesov *et al*. 1989). The Combined Radiometer and Photometer for Mars (KRFM) contained a nadir-pointing, 10-channel, GaAs point spectrophotometer covering the wavelength range 0.32–0.6 μm, and a 5-channel thermal infrared radiometer (Ksanfomality *et al*. 1989). The Imaging Spectrometer for Mars (ISM) was a PbS scanning, imaging spectrometer. An image or "window" was built up by measuring light reflected from a movable mirror that scanned across-track as the spacecraft drifted along-track. For each pixel a spectrum was measured, comprising 64 channels each from the first grating order (1.64–3.16 μm) and the second order (0.76–1.51 μm) (Bibring *et al*. 1989). ISM and KRFM were coaligned to within 0.5°.

TABLE I
Multispectral Data Returned by *Phobos 2*

Instrument and data	Wavelength range	Used/reason not used
VSK: wide-angle images	visible, 0.4–0.6 μm; NIR, 0.8–1.1 μm	Used
VSK: narrow-angle images	broad band, 0.4–1.1 μm	Insignificant spectral information
VSK: spectrometer	35 channels, 0.4–1.1 μm	Insufficient signal levels
KRFM: UV–visible spectra	8 usable channels, 0.328–0.60 μm	Used
KRFM: thermal IR spectra	5 channels, 3–20 μm	Not germane to goals of paper
ISM: 24 × 25 image	128 channels, 0.76–3.16 μm	Used
ISM: 1-pixel wide strip	—	Contamination by Mars in background

All of these devices returned some data from Phobos. In this study we have chosen to use only those parts of the data that cover Phobos with high signal-to-noise data in the UV–visible–NIR wavelength range and that are uncontaminated by stray light from Mars, which was in the background in some of the measurements. The spatial coverage of Phobos by these portions of the data is shown in Fig. 3a. VSK returned 12 pairs of wide-angle images and 13 narrow-angle images. In that the focus of the present study is spectral properties of Phobos, we have used only the wide-angle narrow-band images. Nine of the wide-angle image pairs are usable, i.e., have a relatively good spatial resolution of 260–570 m/pixel and are free of saturation effects. These cover the longitude range 30°–250°W. Three of the nine pairs also show parts of Mars in the background, and were used as described below to validate camera calibration (Avanesov *et al.* 1989, 1991, Murchie *et al.* 1991a).

In the case of KRFM, we have chosen to use only the spectrophotometer data. Eight of its ten channels returned usable measurements of Phobos, i.e., data with a high signal-to-noise ratio. These channels have response functions centered, respectively, at 0.328, 0.346, 0.363, 0.410, 0.445, 0.448, 0.55, and 0.60 μm, and are inherently coaligned. KRFM had a field-of-view (FOV) of $\sim$1 km^2 on the surface of Phobos, and measured 2 groundtracks at 1-sec intervals as the FOV moved westward across the surface of Phobos at a relative velocity of $\sim$43 m/s (white lines, Fig. 3a) (Ksanfomality *et al.* 1991). The first, longer groundtrack also included measurements of Mars, which was in the background of Phobos. These proved critical for accurate calibration of spectra of Phobos. KRFM also conducted 11 measurements sessions of Mars alone, while unobstructed by Phobos.

ISM measured a 1-pixel wide swath and then a 25 × 24 pixel image of Phobos at 700 m/pixel spatial resolution, at the same times when the KRFM groundtracks were measured (Fig. 3a). We have used only the image, because during the measurement of the 1-pixel strip stray light from Mars contaminated the signal from Phobos. ISM, like

KRFM, also conducted 11 measurement sessions for Mars and returned over 36,000 individual spectra. The Mars data, which cover many regions whose properties are known independently from telescopic observations, were used to calibrate the Phobos data.

DATA REDUCTION

Calibration of these data is illustrative of the problems in analyzing data returned from a spacecraft outside of the carefully controlled conditions of a terrestrial laboratory. Such a procedure is workable, as we will demonstrate below, but requires care and sometimes innovative procedures. The VSK cameras were body-fixed and hence unable to view a dedicated calibration target for checking relative response of the two wide-angle channels. KRFM and ISM both contained internal calibration sources, but their stability since prelaunch measurement cannot be demonstrated. However all three instruments observed Mars, whose spectral properties are well known compared to those of Phobos. In addition, albedo estimates of Phobos derived from the VSK imagery agree well with previous estimates. Therefore we have chosen to use Mars as a spectral standard for relative calibration of all three instruments, and to use VSK data to estimate the absolute brightness of Phobos. We believe that previous difficulties in intercalibrating the three data sets arise from using nonstandardized methods, and that using *consistent procedures* on all three data sets should enable us to integrate the data into a composite spectrum covering the full wavelength range of the instruments (0.33–3.16 μm).

The general equation for calibrating Phobos data to Mars is

$$\text{Pho}_{i.\text{cal}} = (\text{Pho}_{i.\text{raw}} - b_i)\frac{\text{Mars}_{i.\text{tel}}}{\text{Mars}_{i.\text{raw}} - b_i}, \qquad (1)$$

where $\text{Pho}_{i.\text{cal}}$ is the calibrated brightness of Phobos in the ith instrument channel, $\text{Pho}_{i.\text{raw}}$ is the raw DN level for

FIG. 3. False color representations of data returned by *Phobos 2*. North is up on all images. (a) NIR VSK images spanning the longitude range observed on Phobos. The intensity of the images is proportional to reflectance, and the hue represents the calibrated visible/NIR color ratio. The polygon of saturated color at upper left represents the location of ISM coverage of Phobos. The two east–west oriented white lines are the locations of KRFM ground tracks. (b) Top: NIR image of Stickney and the region to its west, acquired at a low phase angle of 7.7°. Bottom: Same image, with the bluer unit shown in false color. The correspondence between hue and visible/NIR color ratio is the same as in (a). (c) NIR image of the region of Phobos measured by ISM. Top: False color overlay of the ISM data shows depth of the 1-μm absorption. Bottom: False color overlay shows visible/NIR color ratio measured by VSK, within the area of overlapping coverage by ISM. The correspondence between hue and visible/ NIR color ratio differs from that in (a) and (b).

Phobos in the same instrument channel, $Mars_{i.tel}$ is the telescopic brightness of some "Mars standard area" in that channel, $Mars_{i.raw}$ is the raw DN level for the Mars standard area, and b_i is the magnitude of offset in the ith channel including both dark current and any additional instrumental effects. This procedure assumes that the offset is known

and stable, and that instrument response is linear over the dynamic range covering both Mars and Phobos.

VSK Image Calibration and Analysis

Calibration and validation of the VSK images has been described in detail by Avanesov *et al.* (1991), Murchie

et al. (1991a), and Bell *et al.* (1990). In summary, a first-order or "engineering" calibration was applied to the images, consisting of subtraction of dark current, division by a flat-field image, correction for detector gain and camera exposure time, and division by the solar spectrum. Preliminary visible/NIR ratio images of Phobos were then constructed; color ratios of different spots common to all the image pairs were found to vary between pairs by a small but systematic factor of typically 5% and up to 13%.

An empirical "recalibration" was therefore applied to correct relative colors of different image pairs, using as a standard a known region of Mars observed in the background in one of the image pairs. This procedure is described in detail by Avanesov *et al.* (1991) and Murchie *et al.* (1991a). The Mars standard area, an albedo feature at ~35°S,335°W which is darker than its surroundings, is located well away from the planet's limb and attendant atmospheric effects on surface color. The standard area was measured in the preliminary ratioed image pair, and a multiplicative coefficient was applied to the whole ratio image to equalize the ratio of the standard area with that of a model spectrum convolved to the VSK bandpasses. This yields correct *relative* color for both Mars and Phobos. Recalibration was then extended to image pairs showing Phobos alone, by standardizing visible/NIR ratios of test areas visible in all the Phobos-only image pairs with their recalibrated values in the Mars–Phobos image pair. Among the image pairs showing Phobos, relative colors across the surface were found to be consistent to within ~2%. Formal uncertainty in the absolute color ratio arises from (a) uncertainties in the Mars spectrum convolved into the bandpasses of VSK; (b) uncertainty in the nominal color ratio measured for the Mars standard area; and (c) uncertainty in the relative sensitivities of the visible and NIR VSK channels between image pairs. These combine to yield a formal uncertainty of ±9% in the absolute values of visible/NIR color ratios.

When this procedure was initially applied by Avanesov *et al.* (1991) and Murchie *et al.* (1991a), the Mars standard area was modeled as an average of representative dark-region spectra from McCord *et al.* (1982) (Fig. 4). This yielded a color ratio for Phobos that was, on average, gray and matched the spectrum from Pang *et al.* (1978) in Fig. 2. Later, it was realized that imagery of Mars acquired only ~6 months previously (Pinet and Chevrel 1990) showed the standard area actually to have an intermediate albedo, approximately 2/3 as much brightened relative to the darkest areas as are the brightest areas. Based on the albedo of the standard area, recalibration of VSK images of Phobos to Mars was therefore modified using a spectral model of the standard area as 2/3 bright material and 1/3 dark material (Fig. 4). This yields an absolute value for Phobos color ratios that is redder, but does not affect the magnitude of color *variations* on Phobos. Later, it will
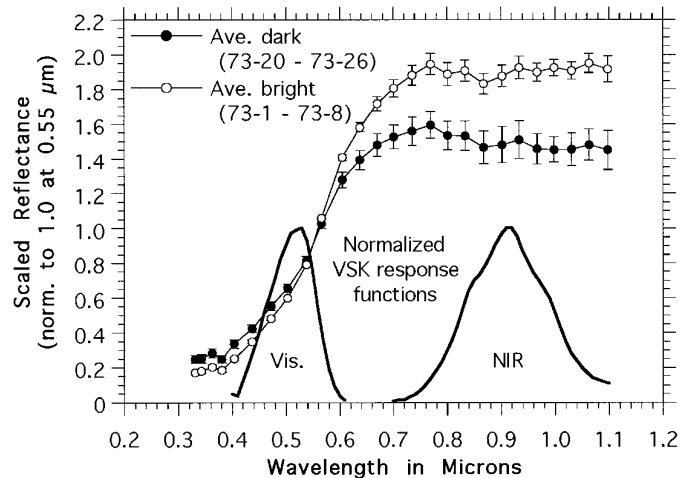

FIG. 4. Normalized frequency response functions of the visible and NIR channels of the VSK camera, shown with the average dark region and bright region spectra used to model the Mars standard area. Data are from McCord *et al.* (1982).

be shown that the consistency of the earlier estimate of Phobos's absolute color with the Pang *et al.* spectrum was misleading, in that the Pang *et al.* spectrum is artificially flat because it mixes measurements of different regions of Phobos shown in the VSK data to have clearly different color properties.

VSK visible–NIR image pairs contain two types of information which are retrievable using different presentations of the data. First, ratio images represented as false color (e.g., Fig. 3a) demonstrate the spatial distribution of color heterogeneities. Second, the image pairs also document the reflectance systematics of different parts of the surface, i.e., how color and albedo variations are related to reflectance in each image channel. Retrieving this information requires standardizing reflectances to a constant viewing geometry to eliminate brightness variations due to illumination. For this purpose, reflectances were measured from 100 shadow-free sample areas 2 × 2 pixels in size in the lowest phase-angle image pair showing Phobos at high DN levels (phase angle 7.7°, to the right in Fig. 3a), and converted into geometric albedo using an appropriate phase function. The results are shown in Fig. 5.

Slightly different phase functions were derived by Avanesov *et al.* (1991) for the visible and NIR channels, using images of Phobos acquired from different perspectives. Figure 5 illustrates the reason for this difference: relatively bluer colors result from increased visible reflectance with little change in NIR reflectance. Additionally, as a result of the *Phobos 2* orbital geometry, the bluer parts of the surface were imaged at low phase angles. Hence at low phase angles the measured visible-channel phase function contains effects of both photometric and color variations. In contrast, the NIR phase function is
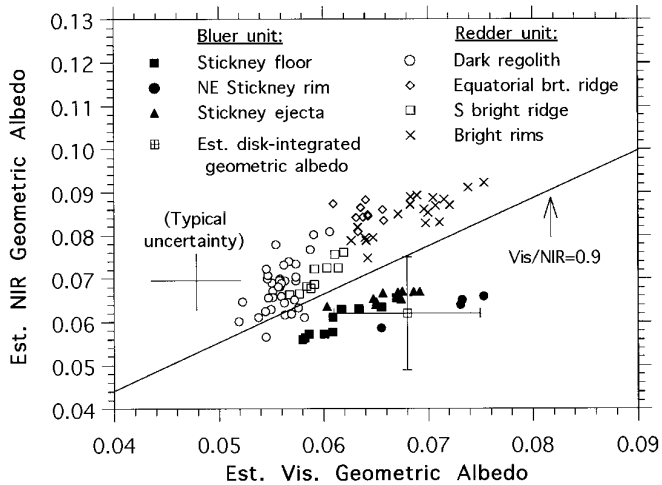
FIG. 5. Reflectance systematics of various geologic features in the bluer unit and redder unit. Each symbol represents average measured reflectances in 4 VSK pixels free of obvious shadows, corrected to 0° phase angle using the phase curve derived by Avanesov *et al.* (1991) for the NIR channel. The estimated disk-integrated geometric albedo is taken directly from Avanesov *et al.* (1991).

dominated by truly photometric effects (Avanesov *et al.* 1991). Therefore both visible and NIR reflectances of the sample areas were converted to geometric albedos using the NIR phase function.

ISM Data Calibration

The procedures used for preliminary reduction and calibration of ISM data have been described in detail previously (Bibring *et al.* 1990, Erard *et al.* 1991). As in the case of the VSK images, a first-order engineering calibration was applied to the data. The first and second order spectra for any pixel each consist of 32 odd and 32 even channels, of which the even channels were used because of their better understood calibration. The data were corrected for dark current measured in-flight, gain measured on-ground, response of the detectors to temperature, and order overlap, and were divided by the solar spectrum. The DN levels thus measured on Phobos were then converted to radiance factors by multiplying by empirical coefficients representing efficiency of the detectors in converting light into signal. Somewhat different spectra have been published by various groups that used different sets of empirical coefficients (Langevin 1991, Bibring *et al.* 1991, Murchie *et al.* 1991b, Murchie and Erard 1993, Murchie and Zellner 1994, Ksanfomality and Moroz 1995).

We recalibrated these data using the same procedure described in Equation (1), with known regions of Mars as a standard, to rederive internal calibration of the ISM measurements of Phobos. Mustard *et al.* (1993) had already applied this procedure to the ISM observations of Mars,

using as standards telescopic spectra of large, homogeneous bright and dark regions of Mars (McCord *et al.* 1982) that were also observed by ISM. In recalibrating the Mars data, Mustard *et al.* derived and applied both gain and offset corrections. These corrections yielded spectra of areas having a variety of albedos that are in excellent agreement with independent telescopic measurements of the same areas (Mustard and Bell 1994), indicating that the corrections are valid and the instrumental gain is linear.

The gain corrections represent the real correction to detector responsivities, and the offsets are generally consistent with expected contributions of martian atmospheric effects and out-of-field stray light (Erard *et al.* 1994). Thus the offsets are inappropriate to the Phobos observations, but the gains alone may contain artifacts of slight inaccuracies in estimation of the offsets for Mars. We therefore minimized such artifacts by fitting Mustard *et al.*'s channel-by-channel gains to yield smooth Phobos spectra, and dividing the Phobos data by the fitted gains. The result is Phobos spectra that are closely similar to those derived by Bibring *et al.* (1991) and Ksanfomality and Moroz (1995). They are however substantially redder than spectra presented by Langevin (1991), Murchie and Erard (1993), and Murchie and Zellner (1994).

Based on the signal-to-noise ratio of the data, the accuracy of the fitting of the channel-by-channel gain corrections, and the close consistency of recalibrated ISM spectra of Mars with well-controlled telescopic spectra (Mustard and Bell 1994), we expect the shape of spectra of Phobos to be accurate to within ±3–4% at the shorter wavelengths. Absolute uncertainty is of order ±10% (Erard *et al.* 1991). Uncertainty of variations *within* the data set is dominated by the signal-to-noise ratio of the data, near 100:1 at 1 μm and 10–15:1 at 3 μm. However, we know of no other published high-quality spectra of Phobos covering the wavelength range of ISM with which to compare our results.

KRFM Data Calibration

Of the three data sets, KRFM has been the most challenging to calibrate. First results from KRFM were calibrated using an internal lamp as a standard, yielding Phobos spectra not greatly unlike previous UV–visible measurements (Ksanfomality *et al.* 1989). Subsequently it was suspected that the calibration lamp was faulty, so the data covering Phobos were recalibrated by standardizing to the disk-integrated UV–visible spectrum presented by Pang *et al.* (1978) and Pollack *et al.* (1978). Results from this procedure were presented by Ksanfomality *et al.* (1991) and Murchie *et al.* (1991a). However, this procedure yielded unreasonable spectra for Mars. Finally, Bibring *et al.* (1991) and Ksanfomality and Moroz (1995) recalibrated Phobos observations by standardizing observations of
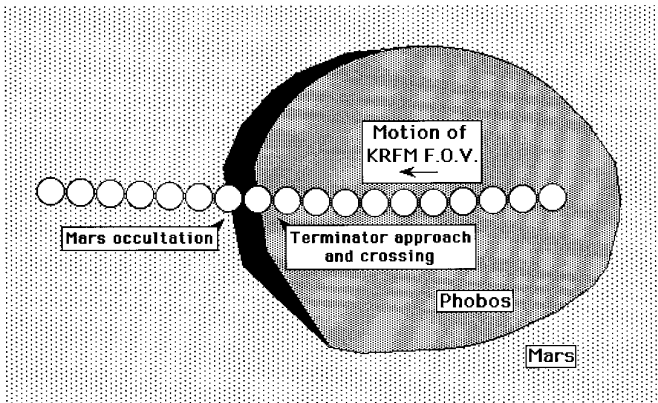
FIG. 6. Geometry of KRFM measurements during and after acquisition of the first, longer Phobos ground track. The instrument field-of-view moved west over the surface of Phobos, into the terminator region, over a thin sliver of the nightside, and onto the illuminated face of Mars in a bright region southeast of Pavonis Mons. As the field-of-view moved onto Mars, it measured spectra of the planet occulted to progressively lesser degrees by Phobos's nightside.

Mars acquired on a different day to telescopic spectra of that planet, using Eq. (1). This procedure yielded Phobos spectra much redder than the results from VSK or ISM.

The conflicting results from earlier attempts to calibrate the KRFM data led us to evaluate the two assumptions of Eq. (1), a known and stable dark current and a linear response over the dynamic range encompassing Mars and Phobos. This was done using observations acquired at the time Mars was observed in the background of Phobos, just after measurement of the first Phobos groundtrack. The geometry of this observation session is shown in Fig. 6. The KRFM field-of-view (FOV) passed from the well-lit, sunward face of Phobos into the terminator region of Phobos where brightnesses decreased rapidly, then over a sliver of the nightside, and then gradually emerged onto the illuminated face of Mars. As the FOV emerged onto Mars, measured brightnesses increased as Mars progressively filled the FOV. VSK and ISM observations both show that the part of Phobos near the terminator is homogeneous spectrally. The part of Mars observed after Phobos is a bright region located several hundred km southeast of Pavonis Mons, which we denote as the ''Mars bright standard area.'' Bright regions throughout this part of Tharsis are also nearly homogeneous spectrally (Murchie *et al.* 1993), and at the wavelengths of KRFM can be modeled using the spectrum of bright regions in Fig. 4.

We first examine the assumption of a known, stable dark current. Three dedicated dark measurements were acquired near the time of measurement of Phobos on March 25, 1989, one on March 21, and two on March 26 (V. Moroz, personal communication). Their magnitudes average approximately 10% of the peak signal from

Phobos, and vary by a factor of two even between the two sets of measurements on March 26. Additionally, one of the two unused KRFM channels returned almost entirely dark current, and that channel shows variations of smaller magnitude over tens-of-seconds periods. Based on these observations, it is our belief that the March 21 and March 26 dark measurements are insufficiently stable for meaningful reduction of the March 25 measurements of Phobos.

Instead, we have estimated the dark current from measurements acquired as the field of view crossed from the illuminated portion onto the nightside of Phobos near the end of the first groundtrack. These are shown in Fig. 7a. If dark currents were absent from the KRFM data, DN levels would have decreased and then increased again proportionately in each channel as the instrument FOV moved through the spectrally homogeneous near-terminator region of Phobos, across the sliver of nightside, and then onto the homogeneous part of Mars. Figure 7a shows that this was not the case; the changes in relative DN levels during the crossing from the illuminated portion onto the nightside of Phobos varied channel-by-channel. The largest relative decrease occurred in the 0.488-μm channel (left half of Fig. 7a). For the purpose of estimating dark currents, we have assumed that offset in the 0.488-μm channel was negligible, and that the lesser changes in DN levels of the other channels resulted from additive components of offset, including dark current. The dark currents may be estimated straightforwardly, by linear regression of the DN level in each channel against that in the 0.488-μm channel (Fig. 7b). The intercepts in Fig. 7b represent offsets b_i in each channel. Although we believe this to be a better estimate of dark current at the actual time of Phobos measurements, it is incomplete because the absolute offset in the 0.488-μm channel is unknown. For this reason we have chosen to reduce further only those measurements acquired from similarly well-lit portions of Phobos (the eastern two-thirds of first groundtrack), to minimize effects of propagated error in dark current removal.

We now examine the assumption of linear response over the brightness range encompassing Mars and Phobos. This assumption may be tested by comparing relative DN levels measured in each channel as Mars progressively filled larger and larger fractions of the instrument FOV, as it came out of occultation by the nightside of Phobos. If gain was linear, then DN levels measured in each channel would be linearly related regardless of the fraction of the FOV filled by Mars. In Fig. 7c the DN level measured in each channel is plotted against DN level in the 0.363-μm channel, which exhibited the overall lowest DN levels while observing Mars. A linear gain is represented by a uniform slope on these plots; nonlinear gain is represented by changes in the slope of the plots with differing brightness. Representative signal levels in each channel are shown for Mars when it filled the FOV (filled circles) and when it
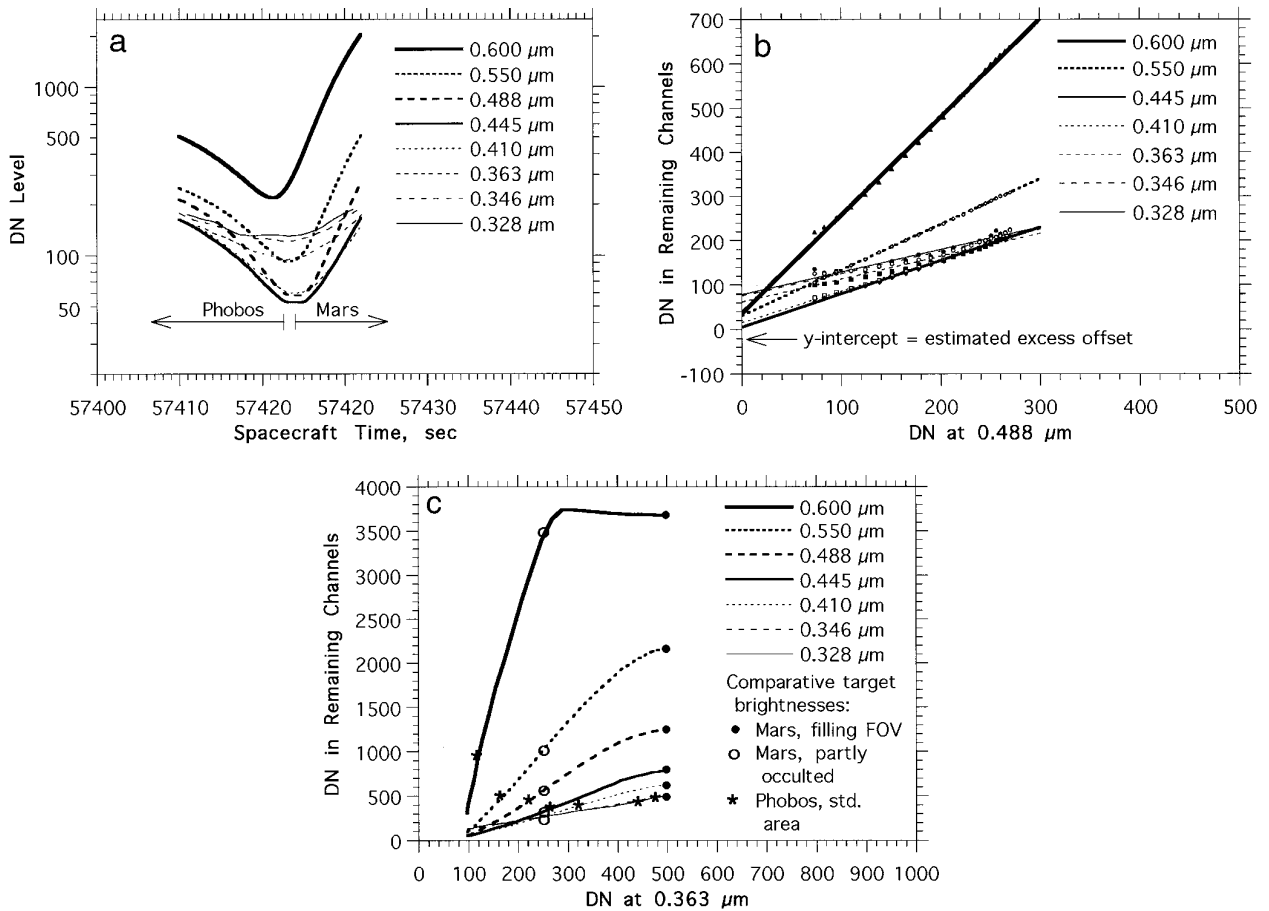
FIG. 7. Variation in the DN levels measured by different KRFM channels before, during, and after traversal of Phobos's night side by the instrument field-of-view. These data allow assessment of the magnitude of offset signal and the linearity of instrumental gain. (a) Variation in DN measured by each channel as the night side was crossed. Note that the lowest DN levels for Mars occur in the 0.363-μm channel, and that the largest decrease in relative DN levels during the crossing from the illuminated portion onto the nightside of Phobos (left half of plot) occurred in the 0.488-μm channel. The lesser decrease in relative DN levels in other channels is inferred to be due to their larger offsets. (b) Comparison of DN level in each channel with DN in the 0.488-μm channel, during traversal of the dimly-lit region near Phobos's terminator (in the central part of Fig. 7a). Each data point represents a pair of DNs measured at one time in two different channels. Each position on the x-axis corresponds to DN measured at one time in the 0.488-μm channel. The data for each channel are fit with the equation for a line. The y-intercept represents the offset in excess of offset in the 0.488-μm channel (which is assumed to be zero). (c) Comparison of DN level in each channel with that in the 0.363-μm channel, as Mars attained greater brightnesses as it came out of occultation. Each position on the x-axis corresponds DN measured at one time in the 0.363-μm channel: for example, Mars when it filled the field-of-view is shown with filled circles, and Mars when partly occulted is shown with unfilled circles. The asterisks correspond only to values on the y-axis, and show DN levels in each channel measured for the Phobos standard area.

was partially occulted by Phobos (unfilled circles). The asterisks denote DN levels for Phobos measured on an eastern portion of the groundtrack, where color properties as measured by VSK are representative of the global average.

In shorter-wavelength channels (0.328 μm to 0.363 μm), the data plotted in Fig. 7b define nearly a straight line; in the longer wavelength channels (0.410 μm to 0.55 μm), the slope of the plots decreases at high brightnesses; and in the longest-wavelength channel (0.60 μm), the plot is nearly flat at high brightnesses. These relationships indicate that gain was linear over the full dynamic range en-

compassed by Mars and Phobos only in the shorter-wavelength channels. In the longer-wavelength channels, gain decreased at higher brightness levels for Mars, and the longest-wavelength channel saturated. Thus it is not possible to calibrate observations of Phobos to unobstructed observations of Mars.

However, KRFM measurements both of Phobos and of Mars *measured during the occultation* (unfilled circles in Fig. 7c) have DN values in the range of linear gain for all channels except the 0.60-μm channel, permitting calibration of those channels of the KRFM Phobos data to observations of Mars *while the planet was occulted*. To do this, we

used the portion of the Phobos groundtrack with globally average color as a "Phobos standard area." The KRFM spectrum of this spot covering the 0.328- to 0.550-μm channels was calibrated to Mars using Eq. (1), with occulted KRFM observations of the "Mars bright standard area" as Mars$_{i.\mathrm{raw}}$, offsets b_i determined as described above, and a spectral model of the "Mars bright standard area" convolved into the KRFM bandpasses (Fig. 4) as Mars$_{i.\mathrm{tel}}$. The resulting spectrum of the "Phobos standard area" was fitted using a second-order polynomial function, to minimize artifacts from errors in gain and offset determinations. The relative reflectance of the Phobos standard area in the 0.60-μm channel was estimated from a linear continuation of the second-order polynomial fit at 0.550 μm. Additional spectral measurements of Phobos were calibrated relative to the "Phobos standard area," so that small spatial variations in relative spectral properties of Phobos would be preserved.

To minimize the effects of the limited knowledge of dark current, we have analyzed here only data from the first two-thirds of the first groundtrack, which is evenly illuminated to within about 20%. Uncertainty in the recalibrated spectra derives from (a) uncertainties in the spectral model of the "Mars bright standard area"; (b) the signal-to-noise ratio of the instrument; (c) uncertainties in the magnitude of the offset removed from the data; and (d) uncertainty in the polynomial fit applied to the "Phobos standard area." Typically, these combine to yield absolute uncertainties of ~10%. Uncertainties in *relative* spectral properties along the groundtrack, dominated by the signal-to-noise ratio of the data and by inaccuracies in dark current removal, are estimated at 1–2% in evenly illuminated areas.

Our recalibrated spectra are actually very similar to spectra of the corresponding locations calibrated against the KRFM internal calibration source (Ksanfomality *et al.* 1989). They are redder than those calibrated against the Pang *et al.* (1978) composite spectrum of Phobos (Ksanfomality *et al.* 1991, Murchie *et al.* 1991a), but substantially less red than spectra calibrated to unobstructed Mars observations (Bibring *et al.* 1991; Ksanfomality and Moroz 1995). The latter difference arises from those groups having used as their standard Mars measurements acquired outside of the domain of linear instrumental response. Later, we will show that KRFM spectra recalibrated in the manner we describe are highly consistent with independent spectral measurements of the same part of Phobos by the *Mariner 9* UVS and by the faint-object spectrograph on the Hubble Space Telescope. It should also be noted, however, that the Principal Investigator of KRFM (L. Ksanfomality) is not in agreement with us on (a) the need for an independent estimate of dark current, or (b) the use of occulted Mars observations from KRFM to obtain Mars calibration measurements that are in the range of linear instrumental response.

Coregistration of Data

Data from the VSK, ISM, and KRFM instruments were coregistered using spacecraft pointing information, augmented by correlation of the brightness features measured by each instrument. Locations of data from ISM and KRFM were first estimated based on spacecraft pointing geometry, and the data were projected onto the VSK images acquired at the same time. (The simultaneously acquired visible–NIR image pair corresponds to the image shown at left in Fig. 3a.) Next, the overlapping wavelength ranges of the instruments were used to check accuracy of this initial coregistration: brightness measured in the longer-wavelength channels of KRFM was compared with brightness measured by the visible channel of VSK, and brightness measured near 0.9 μm by ISM was compared with brightness measured by the NIR channel of VSK.

In the case of ISM, spacecraft pointing geometry yielded a reasonably good correlation between brightnesses measured by the two instruments (Langevin *et al.* 1990). This correlation was improved by distorting the ISM data spatially, to remove effects of slight spacecraft wobble (Langevin 1991). The location of the ISM window on Phobos is depicted in Fig. 3a.

In the case of KRFM, initial track locations were calculated based on location of the ISM window, assuming that the two instruments' optical axes were exactly coaligned. The initial locations yielded correlations with VSK brightnesses of 0.958 for groundtrack 1 and 0.977 for groundtrack 2 (Ksanfomality and Moroz 1995). This correlation is improved to 0.997 for groundtrack 1 and 0.992 for groundtrack 2 by shifting the groundtrack locations northward by ~1.7 km (B. Zhukov, personal communication). This implies that actual alignment of the KRFM and ISM optical axes differed by ~0.4°, which is within the tolerance for the two instruments' coalignment of 0.5°. The revised locations of the two KRFM groundtracks are shown in Fig. 3a. It should be noted that the Principal Investigator of KRFM (L. Ksanfomality) also disagrees with our conclusion that KRFM was not exactly coaligned with ISM.

Data Integration

The final step in data reduction was assembly of composite spectra of portions of Phobos representative of the spectral variation observed across the satellite's surface. A suitable location for this procedure was defined as meeting two criteria: (a) the spectral properties had to be homogeneous locally, to avoid mixing unlike materials if data locations still had minor errors; and (b) it must have been measured by KRFM at a brightness similar to that of the "standard area," to minimize introduction of artifacts due to inaccuracy in removal of KRFM offsets. Two spots meeting these criteria are located along the first KRFM groundtrack, on relatively dark intercrater plains with vis/

NIR color ratios near 0.72 and 0.86. The former spot was covered by all three instruments; the latter was covered only by KRFM and VSK. As is explained below, these two spots are representative of the two spectral units observed on Phobos's surface.

The general procedure for merging data was to scale the different data sets according to the calibrated color ratio of the spot measured by VSK. Spectra measured by KRFM and ISM were each convolved through the appropriate VSK response function (visible for KRFM, NIR for ISM) to yield resampled reflectances of that spot. Where KRFM and ISM data were merged, a nominal reflectance ratio ISM/KRFM was divided by the visible/NIR color ratio measured from recalibrated VSK images, to yield a scaling factor for the two data sets. Where only KRFM data were present, the NIR channel of VSK was used to extrapolate reflectance at NIR wavelengths. Geometric albedo was estimated by scaling to the expected visible-wavelength geometric albedo for typical surfaces having the colors of these spots, 0.06 for the redder spot and 0.055 for the less red spot.

The most difficult step in this procedure is the choice of the VSK color ratio used to merge the data sets, whose formal uncertainty is ±9%. The region of Mars surrounding the standard area contains a mosaic of small darker spots set in a background of brighter, redder material. The low spatial resolution of the telescopic imagery used to estimate the standard area's albedo would have the effect of averaging these differences. In contrast, because of the high spatial resolution of the VSK data, it is possible that VSK measurements of the calibration area represent material that is darker and less red than that represented by the telescopic spectrum. The effect on the calibrated VSK color of Phobos would be to make it appear systematically redder, whereas the real color would be bluer. In merging the data sets we therefore explored two cases, (a) where the nominal color ratio is accurate, and (b) where the real color ratio is one standard deviation bluer than calculated. In reality these two cases probably bracket the range of actual conditions.

RESULTS

VSK Images

Figure 3a shows two representative visible/NIR color ratio images obtained by VSK. The left image was obtained at a sub-spacecraft longitude of ~210°W and a phase angle of 31°, and shows illuminated portions of the surface as far west as the terminator at ~250°W; the right image was obtained at a subspacecraft longitude of ~128°W and a phase angle of 8°, and shows regions as far east as the limb at ~30°W. The "average" color ratio of the surface is near 0.85, but there are spatially coherent local variations of up to −25% and +40%.

Three potential sources of this color heterogeneity are (a) variations in the amount of Marsshine incident on the surface of Phobos, (b) variations in color due purely to photometric geometry, and (c) actual variations in Phobos's surface physical properties. Goguen *et al.* (1979) showed that Marsshine could account for up to several percent of the incident light on the sub-Mars hemisphere, but would be absent from the anti-Mars hemisphere. The typical color ratio of light reflected from Mars is ~0.4, such that Marsshine would cause the sub-Mars hemisphere of Phobos (centered at 0° longitude) to have a color ratio up to a few percent lower ("redder") than the average surface. Figure 3a shows that Phobos's surface actually exhibits the highest ("bluest") color ratios in the sub-Mars hemisphere (270°W–90°W), so that this effect is inconsistent with the observed color heterogeneity. Gradie *et al.* (1980) and Gradie and Veverka (1986) showed that a homogeneous particulate material appears "redder" when observed at higher incidence or emergence angles. If this effect alone was responsible for the color heterogeneities on Phobos, then the visible/NIR ratio should vary regularly with distance from the limb and/or terminator. Examination of Fig. 3a does not reveal this type of variation. Photometric effects on color may well be present in the VSK images Phobos, but they do not account for the observed color heterogeneities. Finally, if the color heterogeneity was due to actual variations in surface physical properties, then color variations might be associated with specific geologic features. Fig. 3a shows that the extreme values of color ratio (the "reddest" and "bluest" surfaces) are associated spatially with specific impact craters. This relationship is clear evidence that variations in Phobos's color are best explained by differences in surface physical properties. The surface has clearly not been homogenized by impact mixing, and the nature and spatial distribution of color heterogeneities contain important information about surface geologic evolution.

The observed portion of the surface may be divided into two basic units based on visible-NIR reflectance properties. One unit, here called the "bluer unit," has a visible/NIR ratio between 0.85 and 1.2, and comprises the "blue" and "bluish gray" materials of Murchie *et al.* (1991a). The bluer unit comprises the interior of the crater Stickney are the surrounding terrain as far west as 160°W. At least three observations suggest that the bluer unit actually represents material excavated and redeposited by Stickney, i.e., ejecta. First, coverage by this unit is continuous within Stickney and adjacent to it. The unit becomes discontinuous and patchy only in its distal portions where it is broken by redder-colored ridges, consistent with removal of the thin distal crater ejecta by mass wasting since formation of Stickney. Second, the bluest-colored material (the "blue" material of Murchie *et al.* 1991a) is exposed in the interior of the crater, specifically on its steep northeast wall. At

this location, mass wasting of any laterally transported, less blue material would be most effective in exposing the bluest-colored substrate. Third, the bluest material outside Stickney's rim occurs as a lobe to the southwest of the crater. Medium-resolution *Viking* images such as Fig. 1a (~100m/pixel) show morphologic evidence at this site for hummocky ejecta deposits that are superposed on the crater rim and spill out beyond it.

The second unit, here called the "redder unit," has a visible/NIR ratio of 0.6–0.85 and occupies the remaining observed portions of Phobos's surface. This unit comprises the "reddish gray" and "red" materials of Murchie *et al.* (1991a). Spatially, the redder unit is more homogeneous than the bluer unit, with most areas exhibiting a visible/NIR ratio of 0.7–0.8. However, dark-floored craters are abruptly different from their surroundings and expose the reddest material observed on the satellite (the "red" material of Murchie *et al.* 1991a).

The reflectance systematics responsible for lateral variations in color and albedo are shown in Fig. 5. The distribution of visible and NIR albedos is highly nonrandom, and reflectances group into two populations which can be separated approximately by a line representing a color ratio near 0.85. One population consists approximately of materials forming the bluer unit, in which NIR albedo is largely invariant but visible albedo varies widely, producing the pronounced color variations of the surface. The second population consists approximately of the redder unit. There is a small amount of color variation, but albedo variations in each channel are substantial and mostly correlated. The higher-albedo surfaces correspond with "bright rims" and "bright ridges." These data therefore show that albedo variations in the bluer and redder unit are of different natures: in the bluer unit they correspond with color variations, and in the redder unit they are largely independent of color variations.

The disk-averaged visible and NIR geometric albedos of Phobos as determined from VSK imagery (Avanesov *et al.* 1991) are also shown in Fig. 5, and approximate the characteristics of the bluer unit. The correspondence of average properties with only one spectral unit is easily understood when considering the geometries at which Phobos's surface was observed: the redder unit was observed mostly at the higher phase angles (mostly 30°–90°), but images acquired at low phase angles (down to <8°) were dominated by the bluer unit. Avanesov *et al.* fit the visible and NIR phase curves independently, so it is natural that the estimated geometric albedo would be dominated by the bluer unit, which covered most of the observed surface in the lowest phase angle images.

The reflectance systematics of Phobos in VSK images also show something important about the albedo variations seen in low phase-angle *Viking* images, whose bandpasses lie within that of the visible VSK channel. Variations in

visible albedo, in *Viking* or VSK images, can be due either to brightened ridges and rims of fresh craters or to color variations. However, strongly elevated NIR albedo appears to be associated exclusively with bright rims and bright ridges. Thus NIR images are needed to identify confidently the purely photometric features, and visible images *alone* are inconclusive in separating color variations from albedo variations that occur without color changes.

In the NIR channel, the bluer and redder units exhibit an abrupt difference in the abundance of brightened ridges and crater rims. The redder unit, which encompasses nearly all of the surface regions imaged at high resolution by *Viking* (≤40 m/pixel), exhibits albedo variations like those described by Thomas (1979): many areas are relatively dark, but higher-albedo materials brightened by 30–40% are exposed on the crests of topographic ridges and on morphologically fresh impact craters. In contrast, the bluer unit is conspicuous by its complete lack of bright rims and bright ridges. This difference in albedo properties of the two units is accentuated in Fig. 3b, where a NIR image is overlaid with false color only where the color ratio is >0.85. The only bright materials in the area immediately west of Stickney occur on a large crater to the northwest (Roche), where the redder unit is exposed in patches on the rim, suggesting removal of overlying bluer material by mass wasting.

The lack of bright rims and bright ridges in the bluer unit is inferred by us to be symptomatic of a basic difference in material properties from those of the redder unit. The bluer unit does contain fewer and less prominent topographic ridges than the redder unit, so a lack of bright ridges in the bluer unit could be attributed simply to differences in topographic relief. However, mapping of both units from *Viking* and VSK images shows that the bluer and redder units *both* contain a comparable density of relatively fresh craters. In the redder unit these generally have bright rims (Avanesov *et al.* 1989, 1991). The lack of bright rims in the bluer unit could result from different material properties, from different crater-forming processes, or from differences in physical modification of the two units by mass wasting. There is no obvious basis for either of the latter two differences, leaving different material properties as the only plausible explanation for the difference in the two units' reflectance properties.

In summary, the attributes of the surface of Phobos revealed by VSK images are listed in Table II. A bluer unit with a visible/NIR color ratio of 0.85–1.2 composes the interior of Stickney and surrounding materials interpreted as the crater's ejecta. NIR reflectance of this unit is low and relatively invariant, but substantial variations in visible reflectance produce color differences of up to 40%. A redder unit with a color ratio of 0.6–0.85 composes the remainder of the surface. Reflectance varies by up to 40%, largely without attendant changes in color, due to

TABLE II
Summary of Spectral Properties of Phobos Surface Units

Attribute	Redder unit	Bluer unit
Vis. albedo of "typical" surfaces	0.06–0.07	0.05–0.06
Vis/NIR	0.6–0.85	0.85–1.2
Bright rims on young craters?	Yes	No
Correlation between color, albedo?	No	Yes
Falloff in reflectance, 0.41 to 0.33 μm	~20–30%	~5–20%
1-μm absorption center	0.95–1.00 μm	?
1-μm absorption strength	0–5%	?
3-μm absorption strength	≪10%	?
Geologic correlation	Remainder of surface	Stickney interior and ejecta

occurrence of brightened materials on topographic ridges and rims of morphologically fresh craters. Locally, the extremes in color are exposed within impact craters. The bluest material is exposed within Stickney and the reddest material composes the low-albedo floors of dark-floored craters.

UV–Visible Spectra

KRFM spectra cover mainly the redder unit, although a few spectra from the eastern portion of the first groundtrack sample the distal portion of the bluer unit (Fig. 3a). Figure 8 shows a representative selection of spectra from the two units. The redder unit is relatively homogeneous spectrally, as also suggested by VSK color ratio images. Its UV–visible spectrum exhibits a consistent smooth red-slope, with an inflection between 0.4 and 0.5 μm. The bluer unit, in contrast, is distinctly different, with an overall lesser spectral slope and the falloff in reflectance into UV wavelengths being less pronounced. These varia-

tions are independent of signal level measured by the instrument, and hence are real properties of the surface of Phobos and not attributable to unrecognized nonlinearity of the instrument or to incomplete removal of dark current.

The difference in UV reflectance properties of the redder and bluer units is illustrated in Fig. 9, where the falloff in reflectance between violet and UV wavelengths is plotted against the visible/NIR color ratio measured by VSK. The redder unit exhibits a UV falloff of 20–30%, largely independent of color ratio. However, the bluer unit exhibits a lesser UV falloff of only 7–15%. This difference and the difference in visible–NIR reflectance systematics support a significant difference in physical properties of the redder and bluer units (Table II).

NIR Imaging Spectroscopy

ISM obtained perhaps the most useful spectral data of the three instruments, because its wavelength range includes absorptions due to Fe near 1 μm and H_2O at 3 μm.
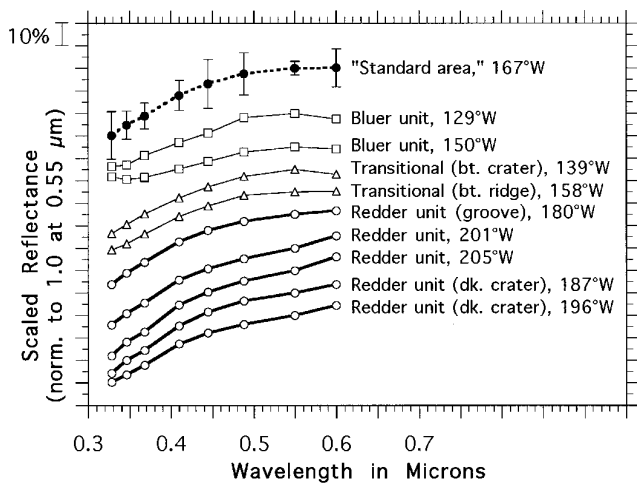

FIG. 8. Selected KRFM UV–visible spectra of Phobos, calibrated as described in the text, covering a variety of geologic features in the bluer and redder units.
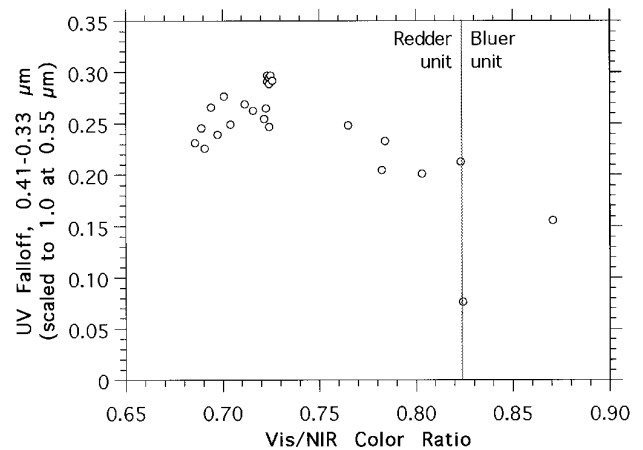

FIG. 9. UV–visible spectral shape measured by KRFM compared with visible/NIR color ratio measured by VSK. The *y*-axis represents the falloff in reflectance from 0.41 to 0.33 μm, which is representative of the magnitude of the UV falloff. The solid vertical line separates visible/NIR color ratios characteristic of the bluer and redder units.
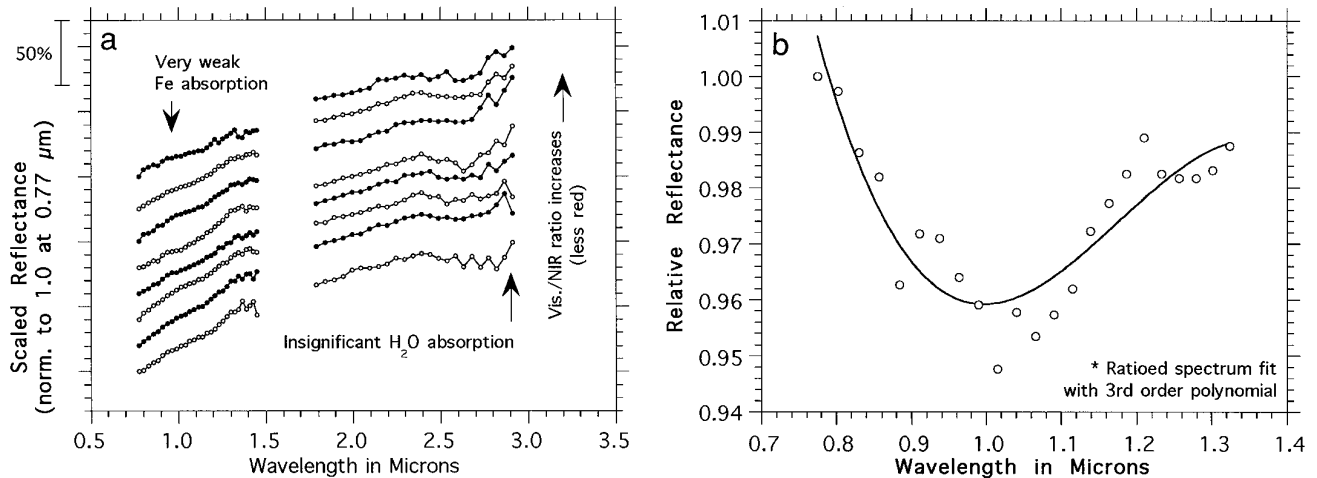
FIG. 10. (a) Selection of scaled ISM spectra from regions having different visible/NIR color ratios as determined by the VSK camera. (b) Ratio of spectra with stronger and weaker 1-μm absorptions, fitted with a polynomial. The band center is at 1.0 μm.

However, spatial coverage by ISM was restricted to the relatively homogeneous redder unit. Representative spectra are shown in Fig. 10a. They are dominated by a nearly smooth red continuum with a weak inflection at 1.4–1.6 μm. No strong mineral absorptions are evident. An increase in reflectance beyond 2.8 μm represents thermal radiation from Phobos's surface, whose temperature at the time of measurement was estimated by the KRFM radiometer to be 260–290° K (Ksanfomality *et al.* 1990).

Potentially the strongest absorptions on the surface of Phobos could be near 3 μm, due to H_2O in hydrated minerals at 2.9–3.1 μm or OH in hydroxylated minerals at 2.7–2.8 μm. Laboratory spectra of a variety of low-albedo meteorite analogs to Phobos show that the H_2O feature exceeds 50% in depth when only $\geq 2\%$ H_2O is present (Salisbury *et al.* 1991). In the representative ISM spectra of Phobos in Fig. 10a, no 3-μm absorption is consistently resolvable above the level of noise in the data. A conservative upper limit to strength of the absorption is therefore $\sim 10\%$. In this way Phobos resembles the other Martian satellite Deimos, which was shown by Bell *et al.* (1989a) to have a similarly weak 3-μm absorption.

The clearest absorption feature present in the infrared is a very weak superposed feature near 1 μm that is evident in several of the spectra in Fig. 10a; strength of the feature varies laterally by several percent. An absorption near 1 μm is characteristic of Fe minerals, and the absorption center is characteristic of the ferrous or ferric phase present (Hunt and Salisbury 1970, Adams 1974, Sherman *et al.* 1982, Morris *et al.* 1985, Cloutis and Gaffey 1991). The small uncertainty in calibration of ISM data make it unwise to assume *a priori* that the band center can be measured directly from these spectra. However, knowledge of variation in the band depth and position *internal to the data* is

limited mainly by the signal-to-noise ratio, which at this wavelength range is nearly $100 : 1$. Therefore we estimated the band center by identifying spectra with similar continua but different strengths of the 1-μm feature, ratioing them, and fitting the result with a polynomial. A typical ratio and its polynomial fit are shown in Fig. 10b. The best-fit band center is ~ 1.0 μm. This wavelength position is inconsistent with ferric-containing phyllosilicate (~ 0.7 μm), which is evident in CM carbonaceous chondrite spectra (Gaffey 1976), or with Fe oxide or oxyhydroxide (Hunt and Salisbury 1970, Sherman *et al.* 1982, Morris *et al.* 1985). Instead this band could result from either pyroxene or a pyroxene–olivine mixture.

The variations in the strength of the absorption were mapped by calculating band depth, using as wings of the absorption reflectances near 0.8 and 1.2 μm, and as reflectance near the band center an average of several channels near 1.0 μm. The resulting map is shown in the upper portion of Fig. 3c. Variations in absorption strength are spatially coherent and non-random, and therefore must be attributable to real variability in light reflected from Phobos and measured by ISM. Three origins of this variability are conceivable: (a) variations in the incident angle of the sunlight (cf. Gradie *et al.* 1980, Gradie and Veverka 1986); (b) contamination of the signal by stray Mars light, which also contains an absorption due to Fe; and (c) actual variations in physical properties of Phobos's surface.

These hypotheses may be evaluated by comparing measured depth of the absorption with reflectance measured by ISM (Fig. 11a) and with visible/NIR color ratio measured by VSK (Fig. 11b). If variations in absorption depth result from photometric geometry, then depth of the absorption should be correlated with measured reflectance of the surface. Figure 11a shows that this correlation is so
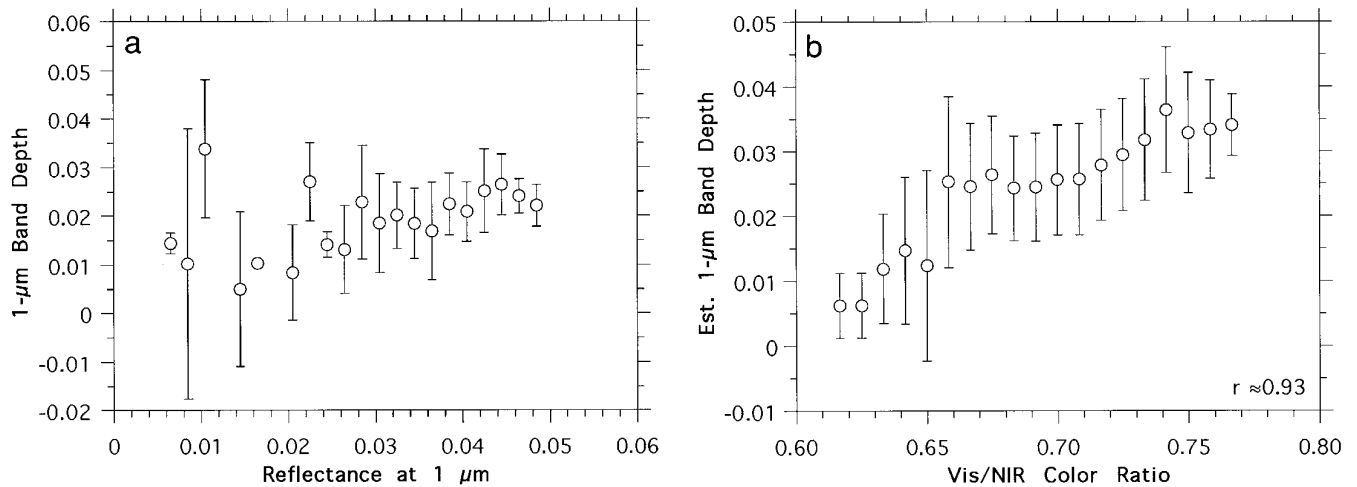
FIG. 11. Comparison of depth of the 1-μm absorption on Phobos with independently measured spectral properties. (a) Absorption depth versus reflectance near 1 μm measured by ISM. Variations in absorption depth due to either scattered Marsshine or photometric geometry would result in a correlation of absorption depth with reflectance. Only ~20% of the variance in absorption depth is related to reflectance, indicating that these effects are minimal. (b) Absorption depth versus visible/NIR color ratio measured by VSK. The high degree of correlation with independently measured color properties indicates that absorption depth variations are related to physical properties of the surface.

low as to be insignificant. If the variations result instead from contamination of the Phobos signal by stray Marsshine, then the absorption should be strongest in poorly illuminated regions of Phobos where stray Marsshine would make the largest relative contribution to measured reflected light. Figure 11a also fails to show this relationship. Finally, if variations in absorption strength are due to real variations in surface properties, then they may correlate with independently measured spectral properties. Figure 11b supports this hypothesis, by indicating that absorption depth is highly correlated with visible/NIR ratio: relatively bluer regions of the surface exhibit a stronger absorption. Figure 3c also shows the spatial variations in visible/NIR color ratio within the area of Phobos observed by ISM. The spatial variations in color ratio correspond closely with spatial variations in 1-μm absorption strength, indicating that variations in each parameter are related either causally or coincidentally.

In summary, the major NIR spectral characteristics of the redder unit are listed in Table I. These include a strong red-slope, a very weak absorption at 1.0 μm, and absence of a significant 3-μm absorption due to H_2O. The strength of the 1.0-μm absorption varies laterally by several percent, and is highly correlated with visible/NIR color ratio.

Composite Spectra

Composite spectra of the bluer and redder units are shown in Fig. 12, representing cases in which nominal VSK color ratios (Fig. 12a) and color ratios one standard deviation bluer than nominal (Fig. 12b) were used to merge the data sets. The spectrum of the bluer unit was constructed

using only KRFM and VSK data, and hence lacks spectral resolution at infrared wavelengths. The spectrum of the redder unit was constructed from all three data sets.

The higher spectral resolution for the redder unit allows assessment of each version of the composite spectra. The spectrum constructed using the bluer than nominal color ratio (Fig. 12b) exhibits smooth red slope within both the KRFM and ISM data, but a strong discontinuity in slope across the intervening wavelength range. In contrast, in the spectrum constructed using the nominal color ratio (Fig. 12a), there is smooth continuity of the continuum slope across the wavelength gaps between the two data sets. This smooth, continuous composite spectrum is graphic evidence that the three *Phobos 2* data sets are well calibrated internally and cross-calibrated to a reasonable degree of accuracy.

DISCUSSION

The *Phobos 2* mission was intended to answer some of the most fundamental questions about Phobos, including its composition, structure, and origin. Loss of the spacecraft before its primary mission was completed prevented these lofty goals from being realized. However, the remote sensing data that were returned, properly calibrated and considered together, either provide partial answers to some of these questions or at least allow recasting of other questions. Considerable space could be devoted to minutiae of these data, but the most important aspects of spatial heterogeneities in color properties and their association with geology have been addressed previously by Ksanfo-
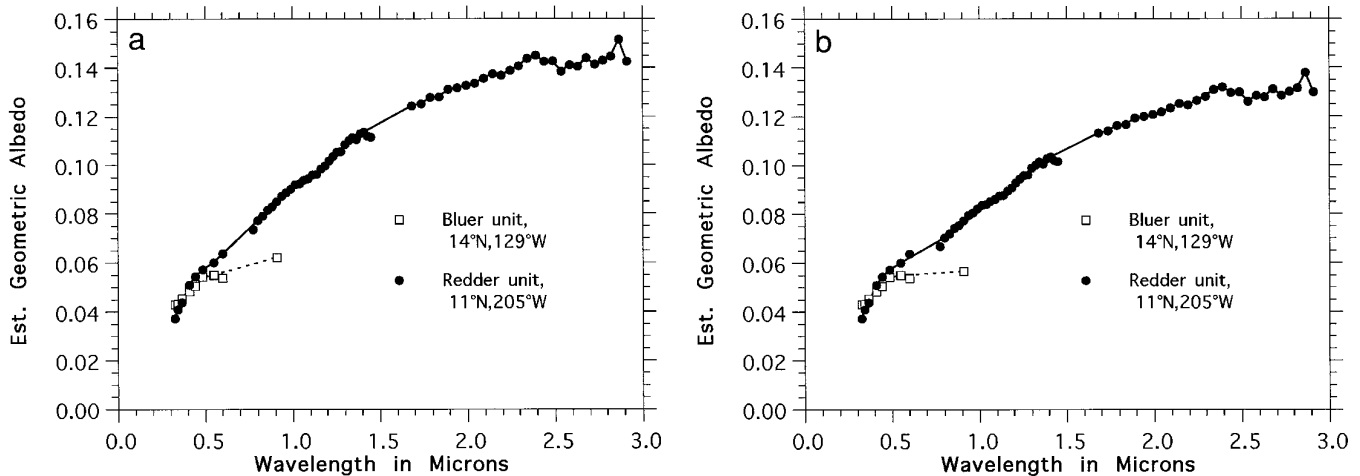
FIG. 12. Composite spectra of the redder and bluer units. (a) Merged assuming the nominal VSK color ratios to be accurate. (b) Merged assuming VSK color ratios to be one standard deviation bluer than nominal.

mality *et al.* (1991), Avanesov *et al.* (1991), and Murchie *et al.* (1991a, 1991b). Below, we frame a discussion of the overall results from the three instruments in the format of seven broad questions particularly relevant to Phobos's geology, its potential as a resource for human space missions, and its future exploration.

(1) Why Do Phobos 2 Data Not Resemble the Pang et al. Composite Spectrum of Phobos?

The composite spectrum presented by Pang *et al.* (1978) (Fig. 2) has driven a great deal of current thought about Phobos, such as the hypothesis of carbonaceous chondrite composition, yet it does not resemble the spectra of Phobos presented here. At the time of Pang *et al.*'s work, the only published assessment of color variations across Phobos's surface (Veverka and Duxbury 1977) stated that color variations were insignificant. In fact, the images those workers used cover mostly the trailing hemisphere, which is blanketed by the redder unit whose relative homogeneity is supported by data from all three *Phobos 2* sensors. But with this assumption in hand, it would be reasonable to assemble a composite spectrum out of whichever data were available.

The notations on Fig. 2 show that the *Mariner 9* UVS data, which form the part of the composite spectrum <0.4 μm in wavelength, cover the leading hemisphere. The *Viking* lander camera data, which form the part of the composite spectrum >0.4 μm in wavelength, necessarily cover the sub-Mars hemisphere. The only coverage of the sub-Mars hemisphere by *Phobos 2* (30°–90°W) was in VSK imagery. That longitude range corresponds with Stickney and its proximal ejecta, which are the bluest materials on the satellite and much bluer (by ~20%) than the average of the leading hemisphere. Thus the Pang *et al.* spectrum consists

of UV data covering a relatively redder region, and visible–NIR data covering a relatively bluer region. We believe that their flat, C-like spectrum at visible wavelengths results from mixing two dissimilar regions of Phobos into a single composite spectrum. The *Phobos 2* data do not resemble that spectrum because it does not really represent the true spectrum of any particular part of Phobos.

(2) Are Phobos 2 Data Consistent with Independent Measurements of Phobos?

The previous discussion underlines the importance to answering this question of comparing only data that cover a single portion of the satellite. The only region of Phobos covered by multiple high spectral resolution, space-based data sets is the leading hemisphere, which is blanketed by the bluer spectral unit. One of these previous data sets is the *Mariner 9* UVS data. The other is a spectrum acquired by the faint-object spectrograph on the Hubble Space Telescope. The FOS also measured other low-albedo asteroids and Deimos at the same time as Phobos, so it is instructive to compare those FOS data with independent measurements first to assess the FOS data's character.

Figure 13a shows the FOS spectrum of the D asteroid 1144 Oda (Zellner and Wells 1994) overlaid on the 8-color spectrum (Zellner *et al.* 1985) of the same body. Assuming that the 8-color data are correct, then the FOS spectrum is in good agreement at 0.3–0.75 μm. Below 0.3 μm the FOS spectrum is very noisy, and beyond 0.75 μm the FOS data are spuriously red. The same conclusion was reached for similar data covering the C asteroid 702 Alauda. We will therefore restrict our comparison of *Phobos 2* and FOS data to FOS data in the wavelength range 0.3–0.75 μm.

Figure 13b shows KRFM, VSK, FOS, and UVS data for the leading hemisphere of Phobos. Allowing for uncer-
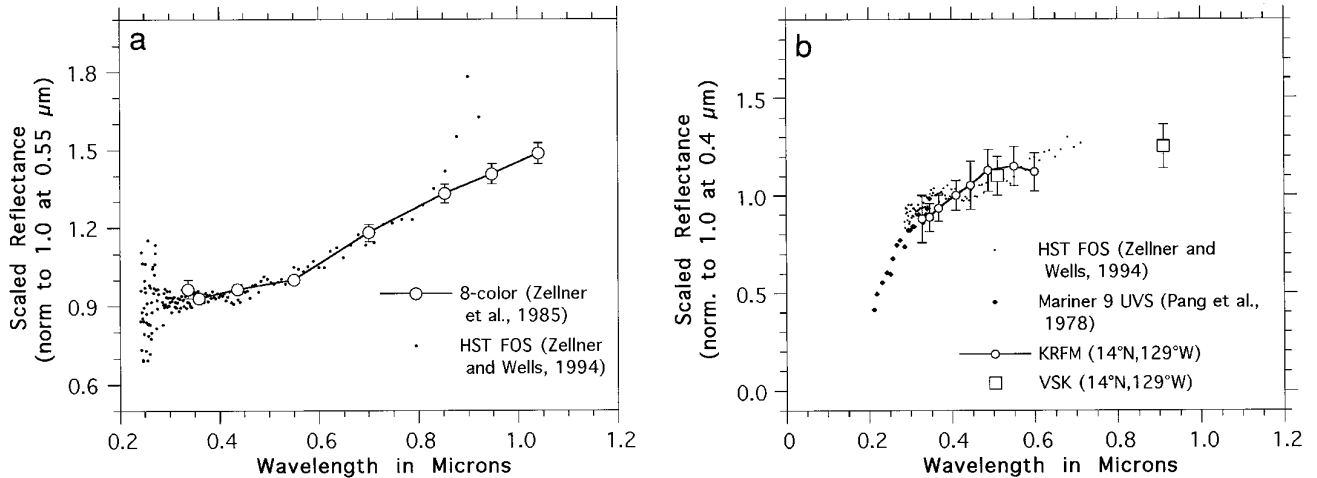
FIG. 13. (a) Spectrum of the D-type asteroid 1144 Oda acquired by the faint-object spectrograph on the Hubble Space Telescope, compared with previous 8-color measurements of the same body. The FOS data agree well in the wavelength range 0.3–0.75 μm. (b) Comparison of space-based spectral measurements of the leading hemisphere of Phobos, which is dominated by the bluer color unit. The independent data sets agree to within their uncertainties.

tainty and noise in the data, all four data sets form a rather smooth, slightly red-sloped spectrum with an inflection at 0.4–0.5 μm, a redder slope at shorter wavelengths, and a grayer spectrum out to 0.9 μm. To within the uncertainty in the data, the *Phobos 2* measurements agree completely with earlier space-based measurements. This result has two important implications for further consideration of the data presented in this paper. First, it shows that the difficult procedure of calibrating KRFM data was successful. Second, it shows that assumptions about the color of the Mars calibration area which are critical to merging the KRFM and longer wavelength (VSK or ISM) data must be approximately correct, or else reflectance from the NIR VSK channel would be inconsistent with the other data sets in Fig. 13b. We may therefore proceed with some confidence in interpreting the compositional significance of the composite Phobos spectra.

(3) What Is the Origin of the Spectral Heterogeneities Observed by Phobos 2?

The arguments presented in various sections of this paper all indicate that the spectral heterogeneities detected by VSK, KRFM, and ISM are caused by intrinsic physical properties of Phobos's surface. There is undoubtedly some effect of photometric geometry and scattered Marsshine on Phobos's color, but these effects do not explain the lateral differences in UV–visible spectral shape, abundance of bright rims on fresh craters, visible/NIR color ratio, or 1-μm absorption depth.

The major intrinsic physical properties of surface materials that could cause spectral heterogeneities are composition, i.e., the relative abundances of major mineral phases

and glasses, and texture, mainly particle size distribution. An origin of Phobos's spectral heterogeneity from simple particle size variations may be evaluated by comparing the spectral variations on Phobos with those produced in the laboratory by comminution of meteorite analogs. Spectral effects of comminution have been examined in ordinary chondrites by Clark *et al.* (1992) and in carbonaceous chondrites by Johnson and Fanale (1973) and Moroz and Pieters (1991). In both types of meteorites, decreased particle size is accompanied by increased albedo at NIR wavelengths with visible albedo remaining more nearly constant, a deepened 1-μm absorption due to pyroxene or olivine, and a reddened continuum slope at visible–NIR wavelengths (or equivalently, a decreased visible/NIR ratio as measured by VSK). In contrast, the redder unit on Phobos exhibits the opposite relationship between absorption strength and visible/NIR ratio: a "redder" color is accompanied by a weakened 1-μm absorption. Thus, simple particle size variations appear inconsistent with spectral heterogeneities observed within the redder unit. Neither can particle size differences simply explain the difference in color and reflectance properties between the redder and bluer units. Particle size variations cause a change in continuum spectral slope as a result of increased NIR albedo; the bluer unit has a less red continuum slope than the redder unit because its *visible-wavelength* albedo is increased relative to its NIR albedo, which remains largely unchanged.

The simplest type of compositional variation on Phobos's surface would be differences in the extent of "space weathering," including melting, comminution, and formation of submicroscopic metallic Fe at grain boundaries.

Clark *et al.* (1992) examined the spectral effects of melting and comminution on ordinary chondrite. They found that this combination of processes, expected from impacts, both reddens continuum spectral slope and decreases strength of the 1-μm absorption. This combination of spectral changes is consistent with internal differences within the redder unit on Phobos. Such processes are also supported by the spatial association of the reddest materials having the weakest 1-μm absorption with dark-floored craters, previously inferred to be sites of impact melting (cf. Goguen *et al.* 1978). However, Phobos may not consist of ordinary chondrite, and melting and comminution alone are not believed to account for "space weathering" on airless bodies.

More direct information on the spectral effects of space weathering on small bodies comes from Galileo observations of 951 Gaspra and 243 Ida. On both asteroids, "fresh" materials exposed by young craters have both a bluer continuum and a stronger 1-μm absorption than does surrounding more "mature" regolith (Belton *et al.* 1992, Granahan *et al.* 1994, 1995). It is appealing to attribute variations in color and 1-μm absorption strength on Phobos, in at least the redder unit, to analogous differences in the extent of "space weathering" of a surface containing mafic minerals. Greater space weathering on Phobos than on a similar-sized asteroid in heliocentric orbit would not be unexpected, because material ejected from Phobos by impacts is trapped in martian orbit and reaccretes in short ($\sim 10^4$ yr) timescales, so that impacts would more or less continue to affect the same surface layer rather than eroding away partly space-weathered material (Soter 1971).

It is equally possible that the variation within the redder unit arises from mixture of two dissimilar lithologies having the same spectral differences as more and less weathered mafic materials. One example is reddish, anhydrous, mafic-poor D asteroid-like material and gray, mafic-rich, black chondrite-like material (cf. Murchie *et al.* 1991a). Such an association would certainly not be expected to have formed together, but could have been brought together by collision of two compositionally distinct protosatellites in Martian orbit.

(4) How Does Phobos Compare, Spectrally and Compositionally, with Other Low-Albedo Small Bodies and with Low-Albedo Compositional Analogs?

It should be clear that the previously believed affinity of Phobos with C asteroids and hence carbonaceous chondrites is based in large part on artifacts in the satellite's previously published composite spectrum, such that this question can now be approached freshly. Because of the more complete spectral coverage of the redder unit, we focus our discussion on that portion of Phobos's surface material.

Figure 14a compares Phobos with representative asteroids from classes that are red, have albedos below 0.12, and are not M asteroids (whose probable metallic composition is inconsistent with Phobos's low density). These include the usual low albedo, red asteroids (C, D, G, and P) as well as K and T types and even the lowest albedo S types. The redder unit on Phobos does not closely match any of these categories. It is much redder than C, G, K, or P asteroids. It is only somewhat redder than D's, but Phobos exhibits a strong falloff in reflectance below 0.5 μm that is lacking in strictly D-type bodies. Overall, among the "conventional" low-albedo asteroids, Phobos most closely resembles T-type bodies, although it is redder than known T-types. Most T's, like Phobos, have a red spectrum, lack strong mafic absorptions, and also lack a 3-μm H_2O absorption (Gaffey *et al.* 1993 and references therein). These are perhaps the most poorly understood class of low-albedo bodies, and have variously been suggested to consist of clay- and carbonaceous-rich material (Bell 1986), troilite-rich material (Britt *et al.* 1992), or physical mixtures of carbonaceous and S-asteroid materials (Gaffey *et al.* 1993).

The spectrum of the bluer unit in Fig. 14a resembles the spectrum of a P-type asteroid, but the wavelength coverage is insufficient for much definitive to be said about this portion of the surface. If the trend of greater flatness at UV wavelengths with bluer color ratios holds out to color ratios typical of Stickney (Fig. 9), then that material might resemble a B- or F-type asteroid spectrally.

Figure 14b shows a comparison of Phobos with laboratory powders of previously proposed meteorite analogs (low- and high-grade carbonaceous chondrites, black ordinary chondrites) (Gaffey 1976). Phobos lacks the sharp inflection at 0.5–0.6 μm and the 0.7-μm Fe absorption characteristic of the low-grade carbonaceous chondrites. The probable position of its 1-μm absorption (1.0 μm) is at a slightly shorter wavelength than that in high-grade carbonaceous chondrites (1.05 μm), whose mafic fractions are strongly dominated by olivine. The band position is longer than that found in black H-type ordinary chondrites (0.90–0.95 μm), but is comparable to that in L- and LL-types (0.96–1.02 μm). However, Phobos appears much redder than any of these materials. This discrepancy is not as important an indicator of composition as the strengths and positions of the 1- and 3-μm bands, however, because unlike the freshly ground meteorite powders Phobos's surface consists of a regolith that probably has been extensively modified by exposure to the space environment.

The low density and low albedo of Phobos have been used as support for the idea that the satellite is a captured, D-like body (e.g., Bell *et al.* 1993). The red continuum of Phobos's redder unit has also been used to support such an affinity with putatively ultraprimitive, very red bodies (Ksanfomality and Moroz 1995). Such
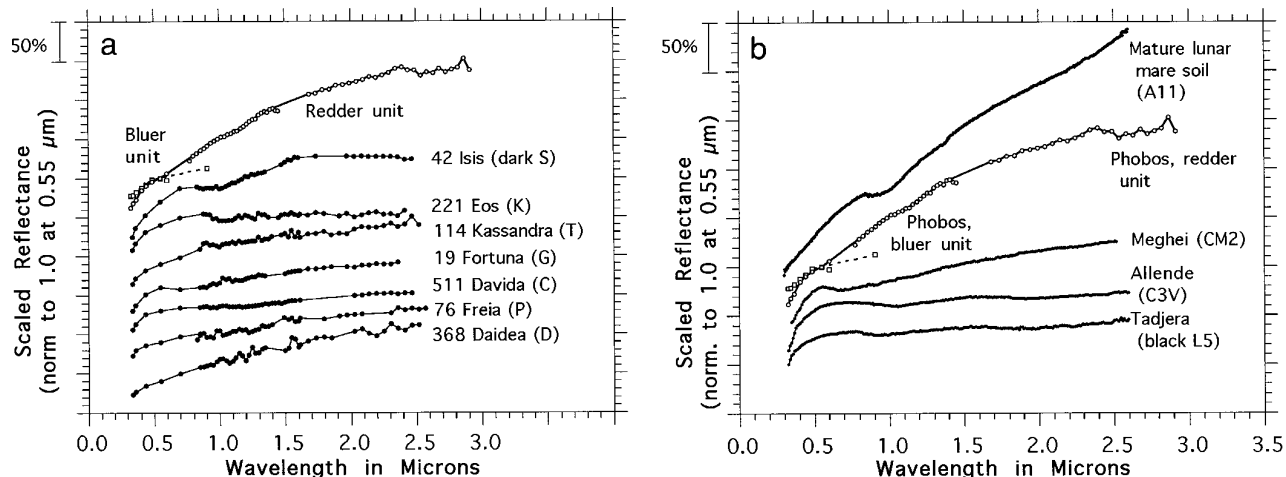
FIG. 14. Comparison of *Phobos 2* spectra with spectra of other low-albedo bodies and low-albedo meteorite analogs. (a) Phobos compared with representatives of low-albedo asteroid classes. The asteroid spectra are arranged with the inferred most mafic-rich types at the top and the more primitive types toward the bottom (cf. Bell *et al.* 1989b, Jones *et al.* 1990). (b) Phobos compared with representative low-albedo meteorite powders and with mature lunar mare soil.

bodies are not believed to have formed at Mars's distance from the sun; if Phobos consists *predominantly* of such material, an origin by capture of an outer solar system interloper is strongly implied. This hypothesis cannot be either proven or disproven with the data presented in this paper. However, Fig. 14b shows that Phobos's continuum is about equally as red as that of mature lunar mare soil, an anhydrous mafic mineral assemblage lacking in organic components. In fact, mature lunar soil provides a better analog to Phobos's redder unit than does any of the asteroid or meteorite analogs thus far discussed, by virtue of its weak 1-μm mafic mineral absorption, UV falloff lacking in D asteroids, utter lack of absorptions due to water, and occurrence at the surface of a regolith that has experienced extensive exposure to space. This comparison is attractive in that it would only require Phobos to be made predominantly of the same minerals that are expected to have formed abundantly at Mars's distance from the sun (e.g., olivine, pyroxene), and does not invoke an exotic overall composition of the satellite (e.g., ultracarbonaceous material) that would probably require an origin as a captured body.

(5) Can Phobos's Surface Material Provide a Source of Water to Human Mars Missions?

A conspicuous characteristic of ISM spectra of Phobos's redder unit (Fig. 10a) is the absence of a 3.0-μm H_2O absorption above the level of noise at this wavelength. Ideally we would like to infer from this observation an upper limit on water content of this spectral unit. Salisbury *et al.* (1991) found that low-albedo CI and CM carbonaceous chondrites contain several percent preterrestrial

H_2O and exhibit a substantial 3.0-μm absorption tens of percentiles in depth. In contrast higher metamorphic grade CO and CV carbonaceous chondrites and ordinary chondrites contain <1% preterrestrial H_2O and exhibit little or no 3.0-μm absorption. Among the population of low-albedo meteorites examined by these authors, 74% of the variance in water content can be fit by the empirical relationship

$$c = 0.106 \exp(6.06\, d), \qquad (2)$$

where c is H_2O concentration in wt. % and d is depth of the 3.0-μm absorption. Phobos's surface consists of a regolith exposed to the space environment, not freshly ground meteorite powders as used by Salisbury *et al.* However, if Eq. (2) still holds for Phobos's surface material and if the upper limit on depth of the 3.0-μm absorption d is taken as ~10%, then the upper limit on water content c of Phobos's redder unit is ~0.2%.

This extremely low upper limit on H_2O content of the redder unit implies one of two conditions. First, the redder unit could consist of a material that was originally rich in water but which has been dehydrated by exposure to the space environment. Second, it could consist of a material which initially contained very little water. The latter would be consistent either with a mafic-rich composition or with a very primitive, ultracarbonaceous, D-asteroid-like composition that never reacted chemically to incorporate bound water (Jones *et al.* 1990).

In any case, the data returned by *Phobos 2* show that at least the redder unit is nearly anhydrous, at the surface, at present. There is no direct evidence for a substantial

reservoir of H_2O on or within the satellite, although such a reservoir could conceivably exist at depth (cf. Fanale and Salvail 1989) or in the bluer unit, depending upon its composition. Until further information reveals direct evidence of such a reservoir, there is no sound basis for planning to utilize Phobos as a source of H_2O or hydrogen for future space missions.

(6) What Is Phobos's Internal Structure?

The data are insufficient to answer this question directly, but three results from the *Phobos 2* mission provide clues. First is the spectral systematics of Phobos's redder unit. There, increasing strength of a mafic absorption at 1.0 μm is accompanied by a redder spectral continuum. As discussed above, either of two different lithologic relationships could explain this. The redder unit could be a mafic mineral-bearing assemblage that is affected to different degrees by space weathering, or it could be a nonuniform mixture of mafic minerals with a reddish, mafic-poor material like that composing D-type asteroids. Unfortunately, lack of high spectral resolution information on the bluer unit prevents it from being related with the redder unit. The bluer unit could simply be richer in mafic minerals, or it could represent a grayer, mafic-poor lithology not evident in the redder unit.

Second is the spatial distribution of Phobos's spectral variations. The extremes of spectral variation are associated with specific impact craters: the bluer unit appears clearly to originate as material excavated by Stickney; the reddest materials compose dark-floored craters within the redder unit. Perhaps the dark-floored craters represent the most space-weathered material rich in porous impact melt, as envisioned by Goguen *et al.* (1978), and the bluer materials excavated from Stickney represent material from depth that has escaped the degree of optical alteration experienced by the redder unit. Alternatively, the bluest and reddest materials might be compositional end-members which dominate the bluer and redder units respectively, as envisioned by Murchie *et al.* (1991a).

Third is the low density, 1.9 ± 0.1 g/cm^3. This value is inconsistent with the density of *any* low-albedo meteorite analog, specifically 2.2–2.3 g/cm^3 for low-grade type CI and 2.6–2.9 g/cm^3 for type CM carbonaceous chondrite, 3.3-3.6 g/cm^3 for higher-grade types CO and CV carbonaceous chondrite, and 3.4–3.8 g/cm^3 for blackened ordinary chondrite (Wasson 1974). Worse yet, the latter meteorite types, which are nearly anhydrous and have mafic mineral absorptions comparable to that of Phobos's redder unit, are the higher in density.

One hypothesis that could account for these seemingly contradictory observations is that (a) the bluer unit excavated by Stickney is representative of most of Phobos's volume, (b) that it is low-density. The low density could arise from a high porosity of a mafic-rich mineral assemblage, or because it consists of some grayish, low-density material like that which may compose B- or F-type asteroids. In either case the redder unit would represent a surface veneer having a thickness of 1–2 km, such that it is penetrated only by the largest impact crater on the satellite (Stickney). The very red floors of dark-floored craters would in this case arise from alteration by the impact process. The redder veneer could have arisen in at least several ways: (a) by the optical alteration a mafic bluer unit to substantial depth; (b) by accretion of D-asteroid like-material onto a mafic bluer substrate; or (c) by accretion of mafic-rich ejecta from martian impact basins, which is later space weathered, onto a bluer and possibly mafic-poor B-, F-, or P-like core. Britt and Pieters (1988) have reviewed the methods by which such an exogenic veneer may have accreted onto Phobos.

Alternatively, Phobos could be a heterogeneous rubble pile consisting of redder and bluer compositional end-members (cf. Murchie *et al.* 1991). In this case the low density would derive at least in part from internal porosity. The redder and bluer end-members would be exposed by Stickney and dark-floored craters, and they would dominate the compositions of the redder and bluer units respectively. The association of stronger mafic mineral absorptions with the bluer unit would imply it in this case to have a mafic-rich composition, and the redder unit would have a more mafic-poor composition.

(7) What Further Measurements are Most Important to Better Understanding Phobos's Composition?

The most immediate benefit for the least effort would come from one or more high-quality UV–visible–NIR spectra of the bluer unit. This would complement existing information on the redder unit and allow the relative properties of these two materials to be better determined. The data could be acquired telescopically from earth, by integrating over the leading hemisphere which is dominated by the bluer unit, or from an instrument in martian orbit or on the martian surface that is capable of resolving the sub-Mars hemisphere sufficiently to pick out the boundary of the two units.

Beyond this, more complete mapping of color properties of the surface at higher spatial resolution ($\leq$50 m/pixel) would allow the detailed comparison of color variations with small-scale geologic features that has been done using *Galileo* imagery of Gaspra and Ida. Even at the 300-m pixel size of the VSK imagery, correlations of color variations with geology are already evident. Significant advances in understanding Phobos could be anticipated from high spatial resolution color imagery of the walls and floor of Stickney, dark-floored craters, and the eastern rim of Stickney and adjacent major grooves not observed by *Phobos 2*.

An ideal remote sensing data set for Phobos would be global, high-spatial resolution imaging spectroscopy out to at least 3.2 μm wavelength. This would allow more complete and finer-scale assessment of the hydration state and Fe mineralogy of Phobos's surface. Perhaps these data, like the color imagery suggested above, could be acquired during an encounter with Phobos of a spacecraft dedicated to observation of Mars.

Ultimately, however, the apparent weakness of absorptions features in Phobos's spectrum is likely to limit the compositional interpretability of remote sensing data. If Phobos's surface composition is currently represented in the meteorite collection, then perhaps spectroscopic measurements or *in situ* analysis of elemental and mineral abundances can identify that material. If it is not represented in the meteorite collection, then only return of a sample to earth is likely to settle definitively the question of the satellite's surface composition.

SUMMARY

In this paper we have rederived the calibration of data from the three multispectral sensors on *Phobos 2* by applying consistent, independently testable methods. We have used the results to characterize spectral heterogeneity on Phobos's surface and to compare the satellite with other low-albedo bodies. The main conclusions of this work are summarized below.

(1) Data from the VSK, KRFM, and ISM instrument are in excellent agreement where their spatial coverages overlap. Where the *Phobos 2* data cover parts of the surface that previously have been measured by space-based sensors, the different data sets are also in agreement.

(2) The 60% of Phobos's surface that was observed by *Phobos 2* is rather heterogeneous and consists of two spectral units. A "redder unit" with a vis/NIR ratio of 0.6–0.85 covers the part of the surface observed at highest resolution in *Viking* orbiter imagery. Its visible-wavelength albedo is typically low, 6–7%. However, the rims on fresh craters are brightened by 30–40% but their color is not distinct from the rest of the unit. Spectrally the redder unit exhibits a strong red slope at all wavelengths, with a steeper slope below an inflection at 0.5 μm. There is a weak Fe absorption near 1 μm, which increases in strength in progressively less red areas. The reddest materials with the weakest 1-μm absorption are exposed in several small, dark-floored craters, which previously have been interpreted as local concentrations of impact melt. There is little or no absorption due to H_2O at 3 μm.

(3) A "bluer unit" with a vis/NIR color ratio of 0.85–1.2 makes up the interior and ejecta of the large crater Stickney. This unit is generally darker at visible wavelengths, with an albedo typically of 5–6%, and it lacks the brightened crater rims typifying the redder unit. However its albedo is higher by almost 40% in the walls of Stickney, where the bluest color occurs. The bluer unit exhibits a much shallower falloff of reflectance into UV wavelengths, but its NIR properties are unknown.

(4) The bluer unit originates from depth, at the site of the Stickney impact. The redder unit represents a widespread shallower layer upon which the bluer ejecta of Stickney is superposed. However, the total depth to which the redder unit extends in regions other than Stickney is unknown, as there are no other exposures of the bluer unit.

(5) None of the observed parts of Phobos has a spectrum resembling a C-type asteroid, like the composite spectrum of Pang *et al.* (1978). However, the origin of that spectrum is easily understood in the context of the lateral heterogeneity of Phobos's color properties.

(6) Only the redder unit is well enough characterized spectrally for detailed comparisons with other low-albedo bodies and with analog materials. It is redder than and distinct from the low-albedo asteroid classes (C and D) with which Phobos has commonly been compared. It is also distinct from most previously proposed meteorite analogs. The closest similarities are with T-type asteroids and with highly space-weathered mafic mineral assemblages.

(7) The weakness of the 3-μm H_2O absorption in the redder unit suggests on upper limit to H_2O content of 0.2 wt. %. There is no direct evidence for a substantial amount of water in Phobos surface, and with existing data that satellite cannot be assumed as a source of hydrogen or water for human Mars missions.

(8) These results do not clearly indicate Phobos's internal structure, but three different hypotheses could explain them. Phobos could consist entirely of porous rubble containing mafic minerals, whose upper horizons are space-weathered and reddened. Alternatively, the surface layer could be reddened instead by intermixture with reddish, anhydrous material such as that composing D-type asteroids. Or the bulk of Phobos could consist of grayish, low-density material like that composing B- or F-types asteroids, overlain by a veneer of mafic-rich material which has become highly space-weathered or is intermixed with reddish D-like material. Narrowing the range of possibilities requires at the least high-quality, high spectral resolution measurements of the bluer unit and the interior of Stickney.

Treiman, and D. Domingue for helpful comments at many stages of this work, and M. Robinson and V. Moroz for careful reviews of the manuscript. Special thanks are due to L. Ksanfomality and V. Moroz for providing KRFM data and extensive discussion on procedures to calibrate them.

REFERENCES

ADAMS, J. 1974. Visible and near-infrared diffuse reflectance spectra of pyroxenes as applied to remote sensing of solid objects in the solar system. *J. Geophys. Res.* **79,** 4829–4836.

AVANESOV, A., B. BONEV, F. KEMPE, A. BASILEVSKY, V. BOYCHEVA, K. CHIKOV, M. DANZ, D. DIMITROV, T. DUXBURY, P. GROMATIKOV, D. HALMAN, J. HEAD, V. HEIFETS, V. KOLEV, V. KOSTENKO, V. KOTTSOV, V. KRASAVTSEV, V. KRASIKOV, A. KRUMOV, A. KUZMIN, K. LOSEV, K. LUMME, D. MISHEV, D. MOHLMANN, K. MUINONEN, V. MURAV'EV, S. MURCHIE, B. MURRAY, W. NEUMANN, L. PAUL, D. PETKOV, I. PETU-CHOVA, W. POSSEL, B. REBEL, YU. SHKURATOV, S. SIMEONOV, B. SMITH, A. TOTEV, YU. UZUNOV, V. FEDOTOV, G.-G. WEIDE, H. ZAPFE, B. ZHUKOV, AND YA. ZIMAN 1989. Television observations of Phobos: First results. *Nature* **341,** 585–587.

AVANESOV, G., B. ZHUKOV, YA. ZIMAN, V. KOSTENKO, V. MURAV'EV, V. FEDOTOV, B. BONEV, D. MISHEV, D. PETKOV, A. KRUMOV, S. SIMEO-NOV, V. BOYCHEVA, YU. UZUNOV, F. KEMPE, B. REBEL, G.-G. WEIDE, D. HALMAN, W. NEUMANN, I. PETUCHOVA, W. POSSEL, J. HEAD, S. MURCHIE, K. LUMME, K. MUINONEN, J. PELTOMIEMI, T. DUXBURY, B. MURRAY, K. HERKENHOFF, F. FANALE, W. IRVINE, AND B. SMITH 1991. Results of TV imaging of Phobos (Experiment VSK-FREGAT). *Planet. Space Sci.* **39,** 281–296.

BELL, J. 1986. Mineralogic evolution of meteorite parent bodies. In *Lunar Planet. Sci. XVIII,* pp. 985–986. Lunar & Planetary Inst., Houston.

BELL, J., M. ROBINSON, T. MCCORD, AND F. FANALE 1990. Comparison of new groundbased and Phobos-2 VSK color ratio data for Mars. In *Lunar Planet. Sci. XXI,* pp. 63–64. Lunar & Planetary Inst., Houston.

BELL, J., PISCITELLI, J., AND L. LEBOFSKY 1989a. Deimos: Hydration state from infrared spectroscopy. In *Lunar Planet. Sci. XX,* pp. 58–59. Lunar & Planetary Inst., Houston.

BELL, J., DAVIS, D., HARTMANN, W., AND M. GAFFEY 1989b. Asteroids: The big picture. In *Asteroids II,* (R. Binzel, T. Gehrels, and M. Matthews, Eds.), pp. 921–945. Univ. of Arizona, Tucson.

BELL, J., F. FANALE, AND D. CRUIKSHANK 1993. Chemical and physical properties of the Martian satellites. In *Resources of Near-Earth Space,* (J. Lewis, M. Matthews, and M. Guerrieri, Eds.), pp. 887–901. Univ. of Arizona, Tucson.

BELTON, M., J. VEVERKA, P. THOMAS, P. HELFENSTEIN, D. SIMONELLI, C. CHAPMAN, M. DAVIES, R. GREELEY, R. GREENBERG, J. HEAD, S. MURCHIE, K. KLAASEN, T. JOHNSON, A. MCEWEN, D. MORRISON, G. NEUKUM, F. FANALE, C. ANGER, M. CARR, AND C. PILCHER 1992. Galileo encounter with 951 Gaspra: First pictures of an asteroid. *Science* **257,** 1647–1652.

BELTON, M., C. CHAPMAN, J. VEVERKA, K. KLAASEN, A. HARCH, R. GREELEY, R. GREENBERG, J. HEAD, A. MCEWEN, D. MORRISON, P. THOMAS, M. DAVIES, M. CARR, G. NEUKUM, F. FANALE, D. DAVIS, C. ANGER, P. GIERASCH, A. INGERSOLL, AND C. PILCHER 1994. First images of asteroid 243 Ida. *Science* **265,** 1543–1547.

BIBRING, J.-P., M. COMBES, Y. LANGEVIN, A. SOUFFLOT, C. CARA, P. DROSSART, T. ENCRENAZ, S. ERARD, O. FORNI, B. GONDET, L. KSANFO-MALITY, E. LELLOUCH, P. MASSON, V. MOROZ, F. ROCARD, J. ROSEN-QVIST, AND C. SOTIN 1989. Results from the ISM experiment. *Nature* **341,** 591–593.

BIBRING, J.-P., M. COMBES, Y. LANGEVIN, C. CARA, P. DROSSART, T. ENCRENAZ, S. ERARD, O. FORNI, B. GONDET, L. KSANFOMALITY, E.

LELLOUCH, P. MASSON, V. MOROZ, F. ROCARD, J. ROSENQVIST, C. SOTIN, AND A. SOUFFLOT 1990. ISM observations of Mars and Phobos: First results. In *Proc. Lunar Planet. Sci. Conf. 20th,* 461–471.

BIBRING, J.-P., Y. LANGEVIN, V. MOROZ, L. KSANFOMALITY, A. GRIGO-RIEV, I. KHATUNTSEV, YU. NIKOLSKY, A. ZHARKOV, AND M. COMBES 1991. Composite KRFM-ISM spectrum of Phobos (0.315–3.1 μm). In *Lunar Planet. Sci. XXII,* pp. 99–100. Lunar & Planetary Inst., Houston.

BRITT, D., J. BELL, H. HAACH, AND E. SCOTT 1992. The reflectance spectrum of troilite and the T-type asteroids. *Meteoritics* **27,** 207.

BRITT, D., AND C. PIETERS 1988. The origin of Phobos: Implications of compositional properties. *Astron. Vestn.* **22,** 229–239.

BURNS, J. 1992. Contradictory clues as to the origin of the martian moons. In *Mars* (H. Kieffer, B. Jakosky, C. Snyder, and M. Matthews, Eds.), pp. 1283–1301. Univ. of Arizona, Tucson.

CLARK, B., F. FANALE, AND J. SALISBURY 1992. Meteorite–asteroid spec-tral comparison: The effects of comminution, melting, and recrystalliza-tion. *Icarus* **97,** 288–297.

CLOUTIS, E., AND M. GAFFEY 1991. Pyroxene spectroscopy revisited: Spectral–compositional correlations and relationship to geother-mometry. *J. Geophys. Res.* **96,** 22,809–22,826.

DUXBURY, T., AND J. CALLAHAN 1989. Phobos and Deimos control net-works. *Icarus* **77,** 275–286.

ERARD, S., J.-P. BIBRING, J. MUSTARD, O. FORNI, J. HEAD, S. HURTREZ, Y. LANGEVIN, C. PIETERS, J. ROSENQVIST, AND C. SOTIN 1991. Spatial variations in composition of the Valles Marineris and Isidis Planitia regions of Mars derived for ISM spectra. *Proc. Lunar Planet. Sci. Conf. 21,* 437–455.

ERARD, S., J. MUSTARD, S. MURCHIE, J.-P. BIBRING, P. CERRONI, AND A. CORADINE 1994. Martian aerosols: Near-infared spectral properties and effects on the observation of the surface. *Icarus* **111,** 317–337.

FANALE, F., AND J. SALVAIL 1989. Loss of water from Phobos. *Geophys. Res. Lett.* **16,** 287–290.

GAFFEY, M. 1976. Spectral reflectance characteristics of the meteorite classes. *J. Geophys. Res.* **81,** 905–920.

GAFFEY, M., T. BURBINE, AND R. BINZEL 1993. Asteroid spectroscopy: Progress and perspectives. *Meteorites* **28,** 161–187.

GOGUEN, J., J. VEVERKA, P. THOMAS, AND T. DUXBURY 1978. Phobos: Photometry and origin of dark markings on crater floors, *Geophys. Res. Lett.* **5,** 981–984.

GOGUEN, J., J. VEVERKA, AND T. DUXBURY 1979. Marsshine on Phobos. *Icarus* **37,** 377–388.

GRADIE, J., AND J. VEVERKA 1986. The wavelength dependence of phase coefficients. *Icarus* **66,** 455–467.

GRADIE, J., J. VEVERKA, AND B. BURATTI 1980. The effects of photometric geometry on spectral reflectance. In *Lunar Planet. Sci. XI,* 357–359. Lunar & Planetary Inst., Houston.

GRANAHAN, J., F. FANALE, M. ROBINSON, R. CARLSON, L. KAMP, K. KLAASEN, P. WEISSMAN, M. BELTON, D. COOK, K. EDWARDS, A. MCEWEN, L. SODERBLOM, B. CARCICH, P. HELFENSTEIN, D. SIMONELLI, P. THOMAS, AND J. VEVERKA 1994. A Galileo multi-instrument spectral analysis of 951 Gaspra. In *Lunar Planet. Sci. XXV,* pp. 453–454. Lunar & Planetary Inst., Houston.

GRANAHAN, J., F. FANALE, R. CARLSON, L. KAMP, K. KLAASEN, P. HEL-FENSTEIN, P. THOMAS, A. MCEWEN, C. CHAPMAN, J. SUNSHINE, M. BELTON, AND THE GALILEO NIMS AND SSI INSTRUMENT TEAMS 1995. Galileo multi-instrument spectral observations of 243 Ida and Dactyl. In *Lunar Planet. Sci. XXVI,* pp. 489–490.

HUNT, G., AND J. SALISBURY 1970. Visible and near-infrared spectra of minerals and rocks. I. Silicate minerals. *Mod. Geol.* **1,** 283–300.

JOHNSON, T., AND F. FANALE 1973. Optical properties of carbonaceous

chondrite and their relationship to asteroids. *J. Geophys. Res.* **78,** 8507–8518.

JONES, T., L. LEBOFSKY, J. LEWIS, AND M. MARLEY 1990. The composition and origin of the C, P, and D asteroids: Water as a tracer of thermal evolution in the outer belt. *Icarus* **88,** 172–192.

KLAASEN, K., T. DUXBURY, AND J. VEVERKA 1979. Photometry of Phobos and Deimos from Viking Orbiter imagers. *J. Geophys. Res.* **84,** 8478–8486.

KSANFOMALITY, L., AND V. MOROZ 1995. Spectral reflectivity of Phobos's regolith in the range 315–600 nm. *Icarus* **117,** 383–401.

KSANFOMALITY, L., V. MOROZ, J.-P. BIBRING, M. COMBES, A. SOUFFLOT, O. GANPANTZEROVA, N. GOROSHKOVA, A. ZHARKOV, G. NIKITIN, AND E. PETROVA 1989. Spatial variations in thermal and albedo properties of Phobos's surface. *Nature* **341,** 588–591.

KSANFOMALITY, L., S. MURCHIE, D. BRITT, T. DUXBURY, P. FISHER, N. GOROSHKOVA, J. HEAD, E. KUHRT, V. MOROZ, B. MURRAY, G. NIKITIN, E. PETROVA, C. PIETERS, A. SOUFFLOT, A. ZHARKOV, AND B. ZHUKOV 1990. Phobos: Spectrophotometry between 0.3 and 0.6 μm and IR-radiometry. *Planet. Space Sci.* **39,** 311–326.

LANGEVIN, Y., J.-P. BIBRING, B. GONDET, M. COMBES, A. GRIGORIEV, B. JOUKOV, AND Y. NIKOLSKY 1990. Observations of Phobos from .8 to 3.15 μm with the ISM experiment on-board the Soviet "Phobos-II" spacecraft. In *Lunar Planet. Sci. XXI,* pp. 682–683. Lunar & Planetary Inst., Houston.

LANGEVIN, Y. 1991. Phobos and other small bodies of the solar system. *Planet. Space. Sci.* **39,** 377–394.

McCORD, T., R. CLARK, AND R. SINGER 1982. Mars: Near-infrared reflectance spectra of surface regions and compositional implications. *J. Geophys. Res.* **87,** 3021–3032.

MOROZ, L., AND C. PIETERS 1991. Reflectance spectra of some fractions of Migei and Murchison CM chondrites and the range of 0.3–2.6 μm. In *Lunar Planet. Sci. XXII,* pp. 923–924. Lunar & Planetary Inst., Houston.

MORRIS, R., H. LAUER, C. LAWSON, E. GIBSON, G. NACE, AND C. STEWART 1985. Spectral and other physiochemical properties of submicron powders of hematite (α-Fe2O3), maghemite (γ-Fe$_2$O$_3$), magnetite (Fe$_3$O$_3$), goethite (α-FeOOH), and lepidocrocite (γ-FeOOH). *J. Geophys. Res.* **90,** 3126–3144.

MURCHIE, S., D. BRITT, J. HEAD, S. PRATT, P. FISHER, B. ZHUKOV, A. KUZMIN, L. KSANFOMALITY, A. ZHARKOV, G. NIKITIN, F. FANALE, D. BLANEY, M. ROBINSON, AND J. BELL 1991a. Color heterogeneity of the surface of Phobos: Relationships of geologic features and comparison to meteorite analogs, *J. Geophys. Res.* **96,** 5925–5945.

MURCHIE, S., S. ERARD, Y. LANGEVIN, D. BRITT, J.-P. BIBRING, J. MUSTARD, J. HEAD, AND C. PIETERS 1991b. Disk-resolved spectral reflectance properties of Phobos from 0.3–3.2 μm: Preliminary integrated results from Phobos 2. In *Lunar Planet. Sci. XXII,* pp. 943–944. Lunar & Planetary Inst., Houston.

MURCHIE, S., AND S. ERARD 1993. The spectrum of Phobos from Phobos 2 observations at 0.3–2.6 μm: Comparison to previous data and meteorite analogs. In *Lunar Planet. Sci. XXIV,* pp. 1025–1026. Lunar & Planetary Inst., Houston.

MURCHIE, S., J. MUSTARD, J. BISHOP, J. HEAD, C. PIETERS, AND S. ERARD 1993. Spatial variations in the spectral properties of bright regions on Mars. *Icarus* **105,** 454–468.

MURCHIE, S., AND B. ZELLNER 1994. The HST spectrum of Phobos:

Comparison with Mariner 9, Viking, and Phobos 2 results. In *Lunar Planet. Sci. XXV,* pp. 957–958. Lunar & Planetary Inst., Houston.

MUSTARD, J., AND J. BELL 1994. New composite reflectance spectra of Mars from 0.4–3.14 μm. *Geophys. Res. Lett.* **21,** 353–356.

MUSTARD, J., S. ERARD, J.-P. BIBRING, J. HEAD, S. HURTREZ, Y. LANGEVIN, C. PIETERS, AND C. SOTIN 1993. The surface of Syrtis Major: Compositions of the volcanic substrate and mixing with altered dust and soil. *J. Geophys. Res.* **98,** 3387–3400.

PANG, K., J. POLLACK, J. VEVERKA, A. LANE, AND J. AJELLO 1978. The composition of Phobos: Evidence for carbonaceous chondrite surface from spectral analysis. *Science* **199,** 64–66.

PANG, K., J. RHOADS, G. HANOVER, K. LUMME, AND E. BOWELL 1983. Interpretation of whole-disk photometry of Phobos and Deimos. *J. Geophys. Res.* **88,** 2475–2485.

PINET, P., AND S. CHEVREL 1990. Spectral identification of geological units on the surface of Mars related to the presence of silicates from earth-based near-infrared telescopic charge-coupled device imaging. *J. Geophys. Res.* **95,** 14,435–14,446.

POLLACK, J., J. VEVERKA, K. PANG, D. COLBURN, A. LANE, AND J. AJELLO 1978. Multicolor observations of Phobos with the Viking Lander cameras: Evidence for a carbonaceous chondrite composition. *Science* **199,** 66–69.

SALISBURY, J., D. D'ARIA, AND E. JAROSEWICH 1991. Midinfrared (2.5–13.5 μm) reflectance spectra of powdered stony meteorites. *Icarus* **92,** 280–297.

SHKURATOV, YU., A. BASILEVSKY, B. ZHUKOV, M. KRESLAVSKY, AND S. MURCHIE 1991. A possible interpretation of bright features on the surface of Phobos. *Planet. Space. Sci.* **39,** 341–347.

SHERMAN, D., R. BURNS, AND V. BURNS 1982. Spectral characteristics of the iron oxides with application to the Martian bright region mineralogy. *J. Geophys. Res.* **87,** 10,169–10,180.

SOTER, S. 1971. *The Dust Belts of Mars.* Center for Radiophysics and Space Physics Report 462, Cornell University.

THOMAS, P. 1978. The *Morphology of Phobos and Deimos.* Center for Radiophysics and Space Physics Report 693, Cornell University.

THOMAS, P. 1979. Surface features of Phobos and Deimos. *Icarus* **40,** 223–243.

THOMAS, P., J. VEVERKA, J. BELL, J. LUNINE, AND D. CRUIKSHANK 1992. Satellites of Mars: Geologic history. In *Mars* (H. Kieffer, B. Jakosky, C. Snyder, and M. Matthews, Eds.), pp. 1257–1282. Univ. of Arizona, Tucson.

VEVERKA, J., AND J. BURNS 1980. The moons of Mars. *Ann. Rev. Earth Planet. Sci.* **8,** 527–558.

VEVERKA, J., AND T. DUXBURY 1977. Viking observations of Phobos and Deimos: Preliminary results. *J. Geophys. Res.* **82,** 4213–4223.

VEVERKA, J., M. MALIN, S. MURCHIE, J. BELL, C. CHAPMAN, L. McFADDEN, M. ROBINSON, AND P. THOMAS 1995. Asteroid 433 Eros: High resolution imaging and spectral mapping from NEAR. In *Lunar Planet. Sci. XXVI,* pp. 1447–1448. Lunar & Planetary Inst., Houston.

WASSON, J. 1974. *Meteorites: Classification and Properties.* Springer-Verlag, New York.

ZELLNER, B., D. THOLEN, AND E. TEDESCO 1985. The eight-color asteroid survey: Results for 589 minor planets. *Icarus* **61,** 355–416.

ZELLNER, B., AND E. WELLS 1994. Spectrophometry of the Martian satellites with the Hubble Space Telescope. In *Lunar Planet. Sci. XXV,* pp. 1541–1542. Lunar & Planetary Inst., Houston.